

Application of scintillation detectors in cosmic experiments

Anatoly Iyudin

Skobeltsyn Institute of Nuclear Physics
Moscow State University by M.V. Lomonosov

ISMART-2018, Minsk (RB), 09-12 October, 2018

Abstract

Scintillation detectors (SDs) based on application of organic plastic scintillators (OPSs), or of inorganic scintillators (IOSs), are widely used in modern space physics, and, generally, in cosmic experiments.

Here we review different detection techniques, as well as technologies for production of OPS and of IOSs different shapes, like strips and tiles (extrusion, injection molding, etc.), optical and physical characteristics of scintillators, and methods of light collection based on the use of direct optical contact, or of wavelength-shifting (WLS) fibers to couple scintillators with different type photosensors.

Examples are given of the use of SDs in the historically and physically important past cosmic experiments, as well, as of modern experiments planned to be carried-out in space, or of ground-based SDs arrays, developed for astro-particle and gamma-ray experiments aimed to search for new (astro)-physics, like new states of matter, antiparticles, neutrino oscillations, and to study astrophysical phenomena and cosmic particles in a wide mass and energies range.

Scintillation detectors hold great promise for future space and ground-based cosmic experiments due to their ability to high segmentation, radiation hardness, possibility to apply WLS fiber light collection and multipixel Si-PM readout.

Especially we'll discuss our experience in application of the new scintillator Ce:GAGG in pixellated gamma spectrometer elaborated in the frame of Russia – Belarus collaborative project.

1903

“The Emanations of Radium.” By Sir WILLIAM CROOKES, F.R.S.
Received March 17,—Read March 19, 1903.

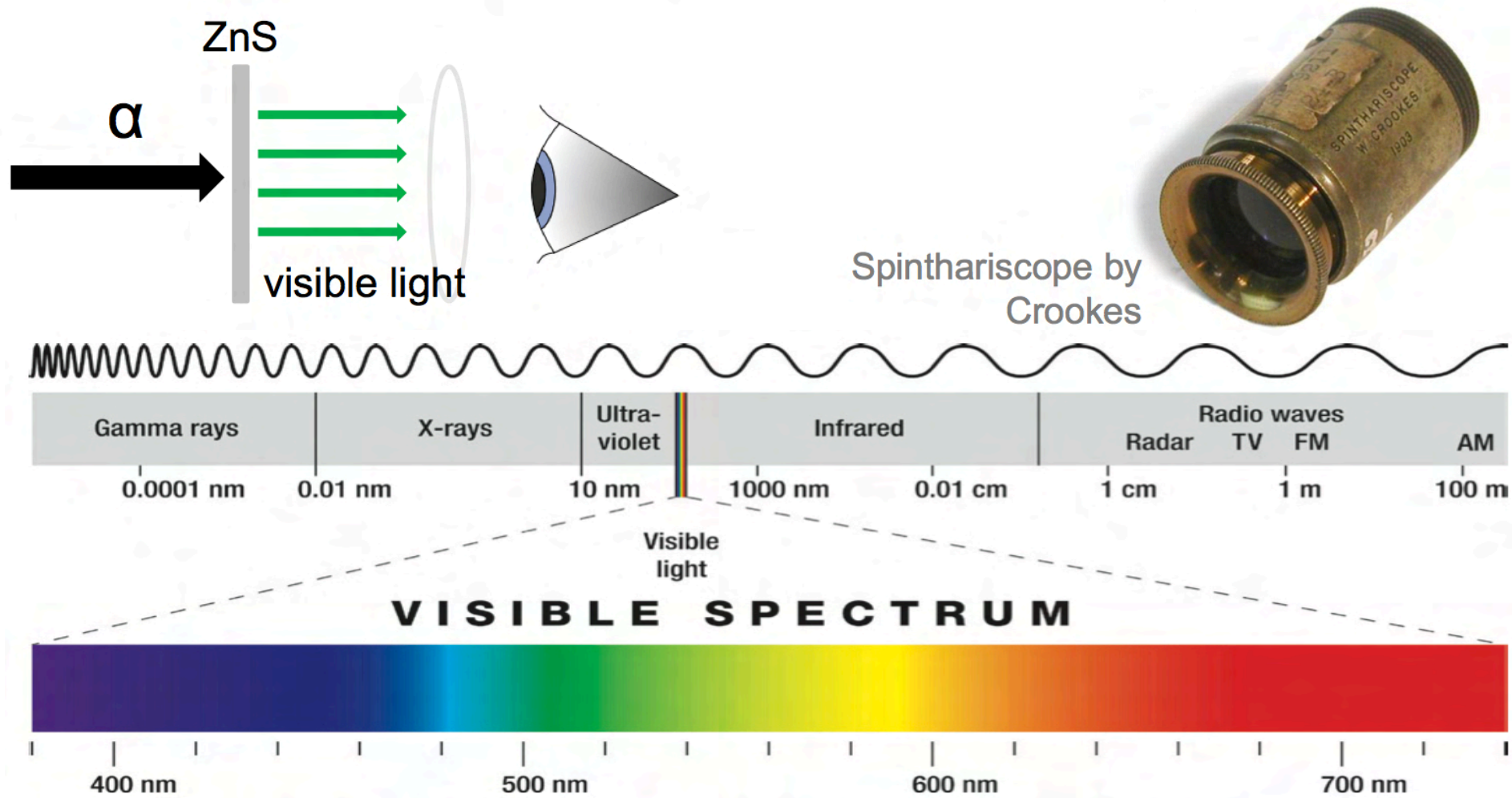


Fig. 1. Electromagnetic spectrum (after <https://luxes.es/basics-of-lighting/?lang=en>)

ISMART-2018, Minsk (RB), 09-12 October, 2018

Next steps

● 1903 “The Emanations of Radium.” By Sir WILLIAM CROOKES, F.R.S.
Received March 17,—Read March 19, 1903.

● 1944 **A PHOTOELECTRIC ALPHA PARTICLE DETECTOR**

● 1948 *Die Fluoreszenzanregung von festem und flüssigem Naphthalin,*

● 1948 **Alkali Halide Scintillation Counters**

ROBERT HOFSTADTER

Princeton University, Princeton, New Jersey

May 20, 1948

**Detection of X-Rays by Means of NaI(Tl)
Scintillation Counters***

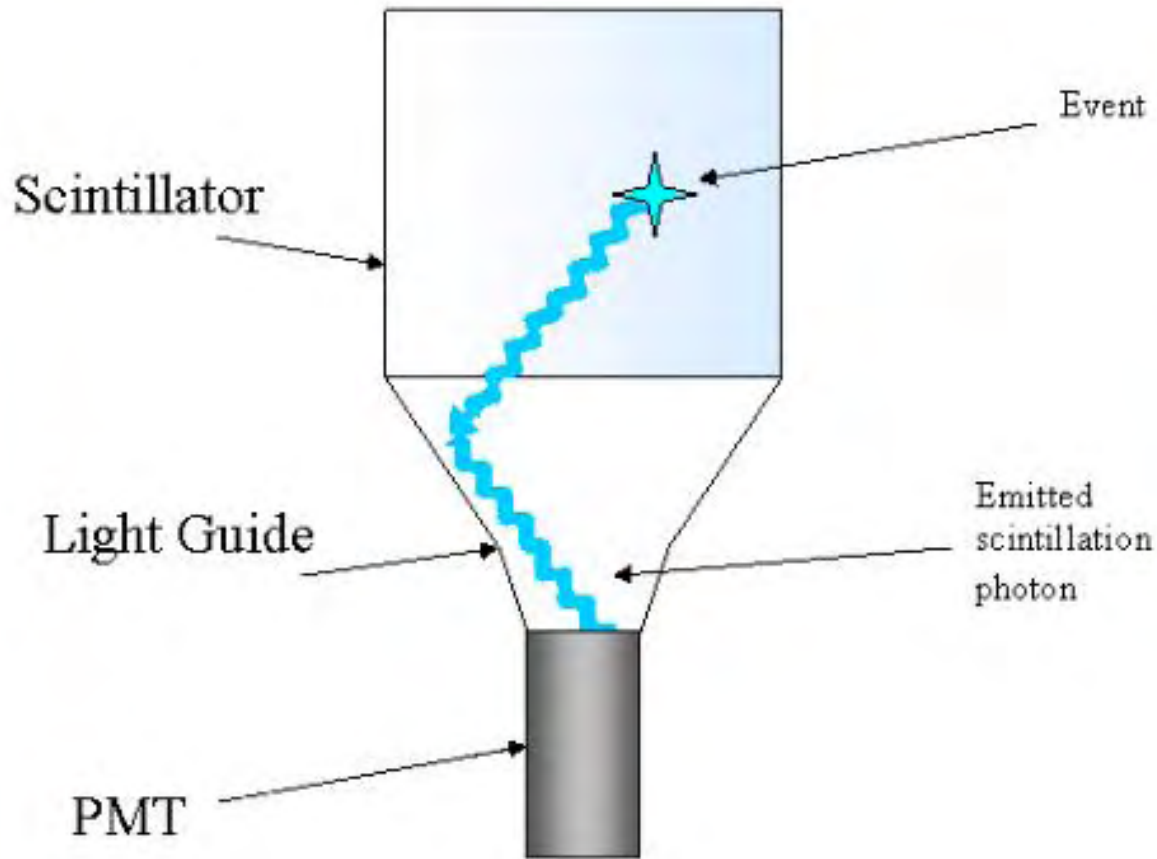
H. I. WEST, JR., W. E. MEYERHOF, AND R. HOFSTADTER

Stanford University, Stanford, California

November 6, 1950

ISMART-2018, Minsk (RB), 09-12 October, 2018

What are Scintillation Detectors?



PMT-a clue to success of scintillating detectors

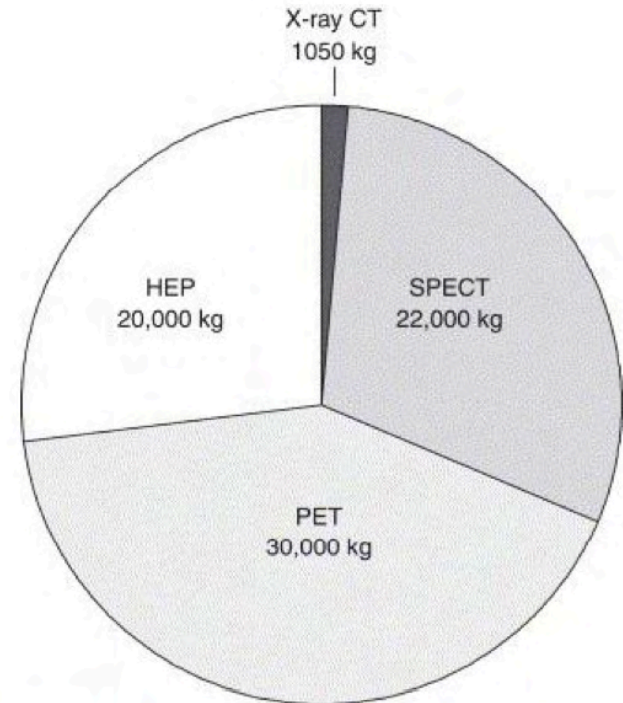
Who are interested?!

Drivers of further scintillator development

- High-energy particle physics (HEP)
- Nuclear Physics
- Neutron physics

Space science

- Medical imaging
 - Medical imaging positron emission tomography (PET)
 - single photon emission-computed tomography (SPECT)
 - X-ray-computed tomography (X-ray CT)
 - Planar X-ray screens



Estimated quantities of scintillators used in 2003 for PET, SPECT, HEP, and X-ray CT (powder phosphor material used in planar X-ray screens is not included.)

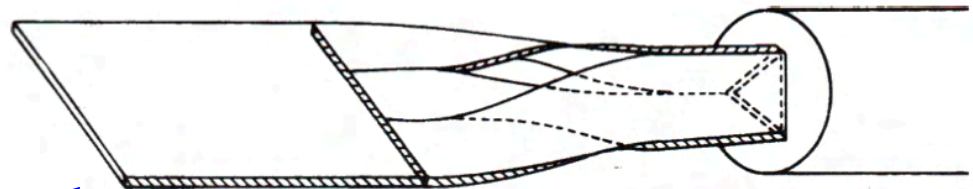
Typical organic, plastic and liquid scintillators

Scintillator	Light Output [% of NaI(Tl)]	Decay Time [ns]	Density [g/cm ³]
NaI(Tl)	100	230	3.67
Anthracene	44	30	1.25
Stilbene	21	4.5	1.16
Plastic (BC-400)	28	2.4	1.03
Plastic (BC-404)	29	1.8	1.03
Plastic (BC-422Q)	11	0.7	1.03
Liquid (BC-501A)	34	3.2	0.87
Liquid (BC-505)	35	2.5	0.87

Organic scintillators

Types of organic scintillators:

- **Plastic** (polymerized solutions)
 - + every form and size possible (fibers, rods, blocks)
 - + easy to produce and handle
 - + large volumes inexpensive
- **Thin films** ($\approx 20\mu\text{g}/\text{cm}^2$)
 - + particle transmission detectors
- **Loaded organics**



Loaded by B, Li, Gd, and by other elements

Inorganic scintillators

Used as central detector, and/or as elements of anticoincidence shield

Scintillator	Light Output [% of NaI(Tl)]	Decay Time [ns]	Density [g/cm ³]	Hygroscopic
NaI(Tl)	100	230	3.67	y
CsI(Tl)	45	680, 3340	4.51	s
CsI(Na)	85-110	460, 4180	4.51	y
CsI(pure)	5	2, 16	4.51	s
BGO	20	300	7.31	n
CdWO ₄	30-50	1100, 14500	7.90	n
CaWO ₄		800	6.10	
ZnS(Ag)	130 (α)	200	4.09	n

Inorganic scintillators

Typical inorganic scintillators:

- **BGO** (Bismut Germanate $\text{Bi}_4\text{Ge}_3\text{O}_{12}$)
 - + high density and Z
 - + largest interaction probability per volume
 - + easy to handle and use
 - low light yield at room temperature
- **Other Crystals:**
 - CdWO_4 , CaWO_4 ,
 - $\text{CaF}_2(\text{Eu})$, $\text{SrI}_2(\text{Eu})$,
 - BaF_2 ,
- **Non-crystal scintillators:**
 - Ceramics / Glasses
 - Noble Gas



BGO Shield – Veto for HPGe

SPI-Integral; DAMPE

Review

Inorganic scintillating materials and scintillation detectors

By Takayuki YANAGIDA*^{1,†}

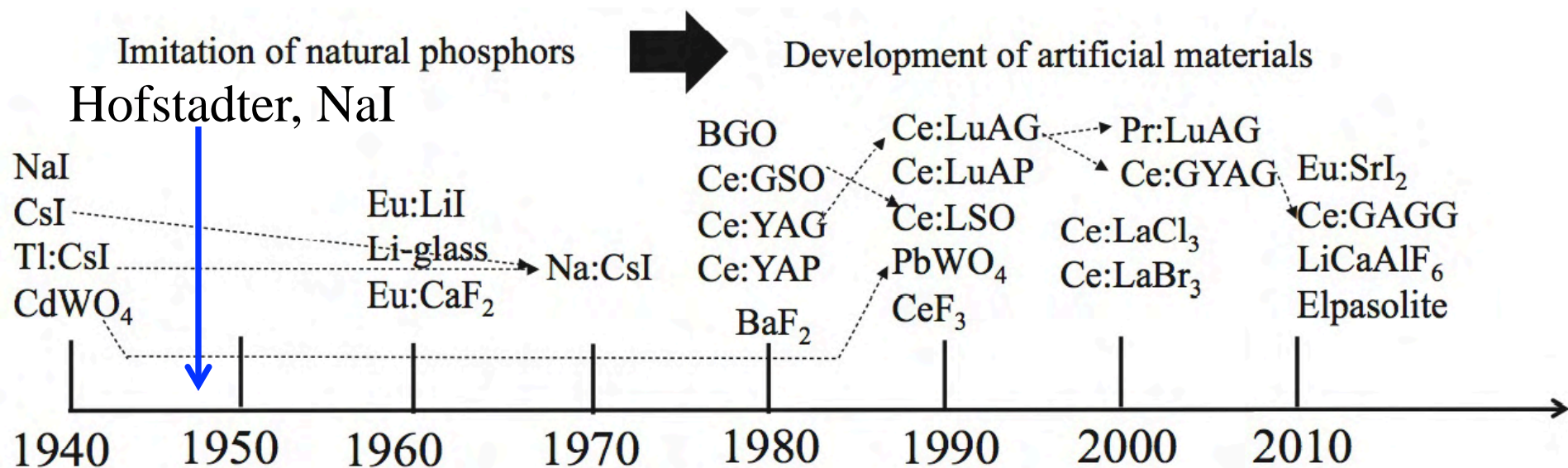


Fig. 8. R&D History of common scintillators. Arrows indicate modifications of materials.

New scintillators

First Generation scintillators

NaI(Tl): energy resolution of 7% at 662 keV, strong non linearity, bad time resolution

BaF₂: bad energy resolution, excellent time resolution

BGO: bad energy resolution, bad time resolution, excellent efficiency

CsI(Tl): good for the measurement of light charged particles

Second Generation scintillators

Lanthanum Halide: **LaBr₃:Ce**, **LaCl₃:Ce**

New Materials: **SrI₂:Eu**, **CeBr₃**

Elpasolide : **CLYC:Ce**, **CLLB:Ce**, **CLLC:Ce**

Ceramic: **GYGAG:Ce**

Material	Light Yield [ph/MeV]	Emission λ_{\max} [nm]	En. Res. at 662 keV [%]	Density [g/cm ²]	Principial decay time [ns]
NaI:Tl	38000	415	6-7	3.7	230
CsI:Tl	52000	540	6-7	4.5	1000
LaBr ₃ :Ce	63000	360	3	5.1	17
SrI ₂ :Eu	80000	480	3-4	4.6	1500
CeBr ₃	45000	370	<5%	5.2	17
GYGAG:Ce	40000	540	<5%	5.8	250
CLYC:Ce	20000	390	4	3.3	1 CVL 50, ~1000

Pulse Shape Discrimination (PSD)

- Technique used to discriminate between signals of different types of radiation.
 - E.g. gamma and neutron events.

- Organic scintillator:
 - Fast (prompt fluorescence) and slow (delayed fluorescence) characterize a pulse.
 - Fraction of light in slow component depends on nature of incoming particle.
 - Slow component depends on rate of energy loss $\frac{dE}{dx}$. Greater for particles with large $\frac{dE}{dx}$.

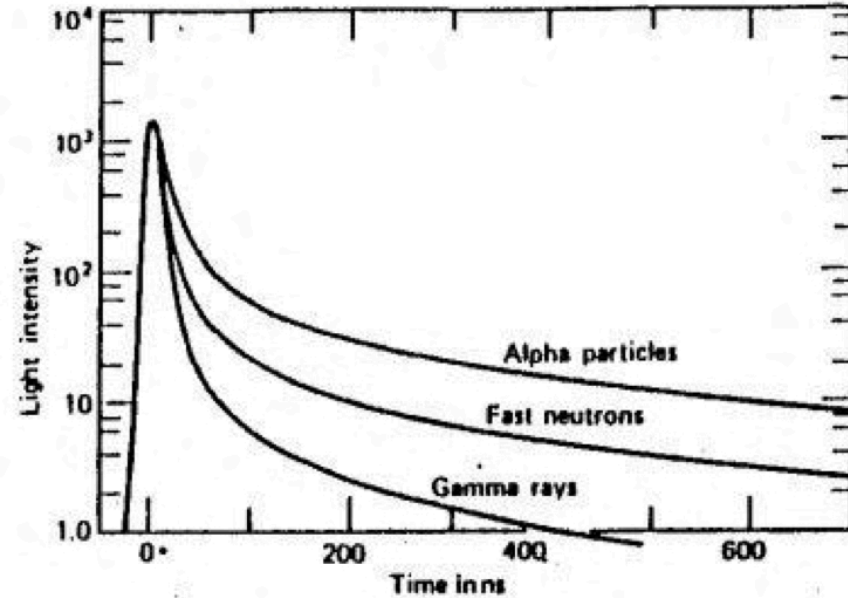
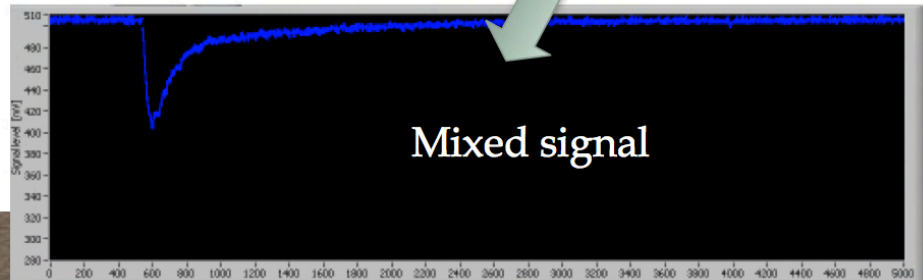
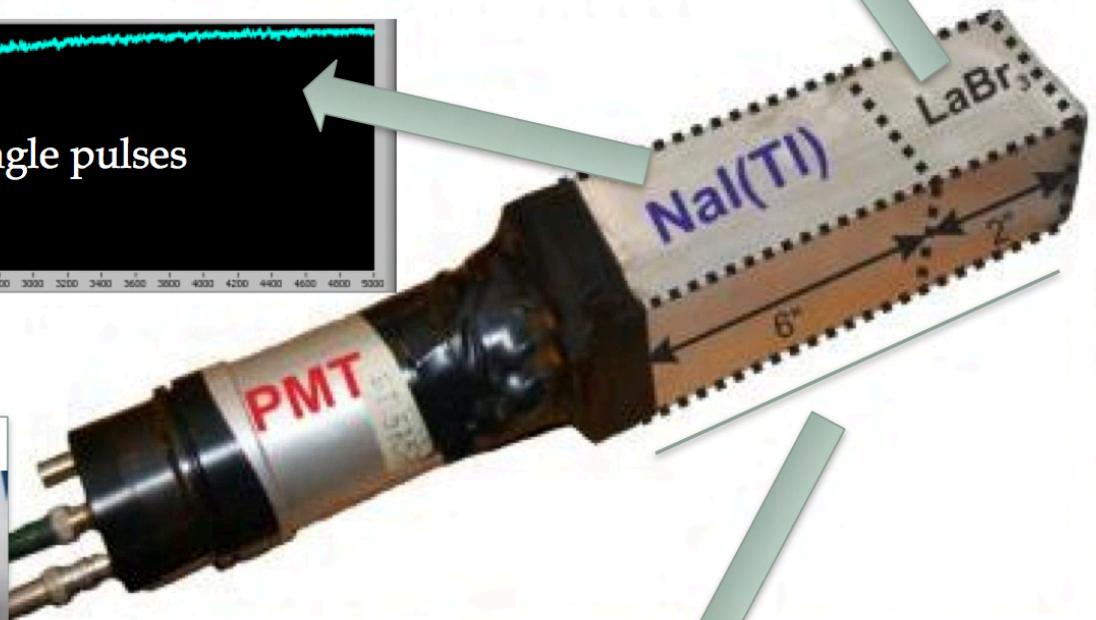
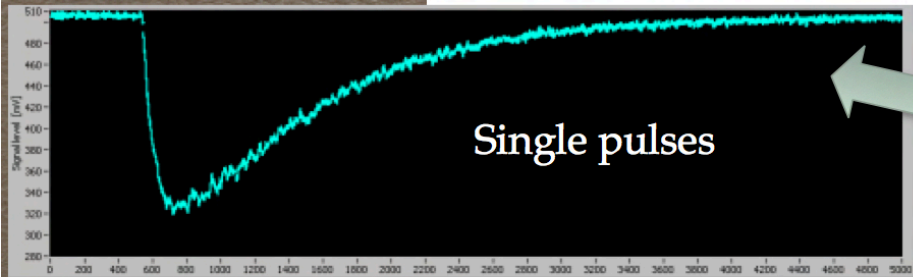
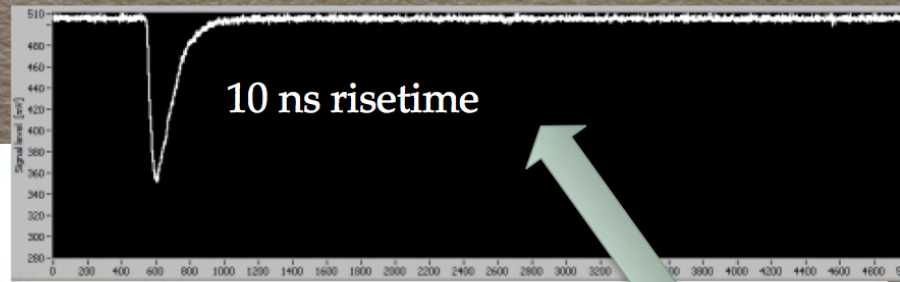
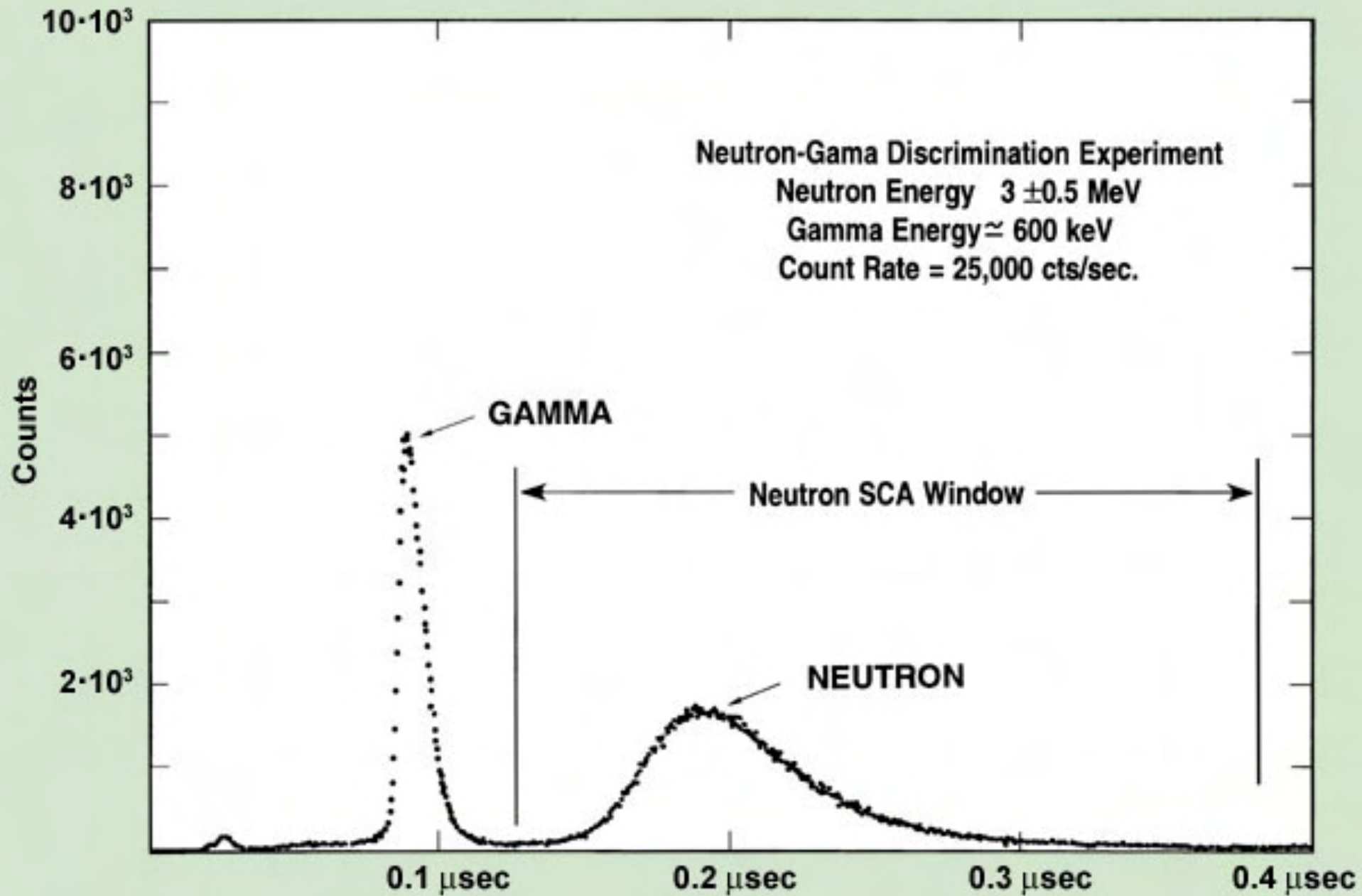


Image from Knoll, G. *Radiation and Detection Measurement*. p. 227.

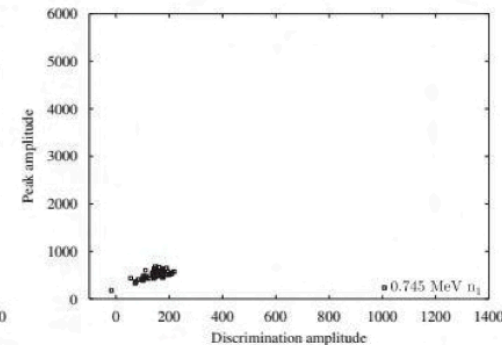
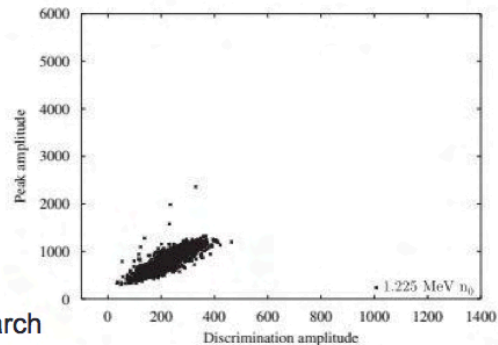
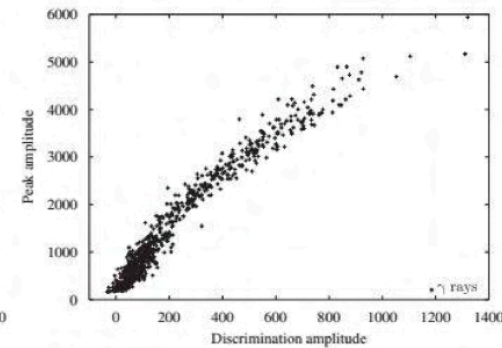
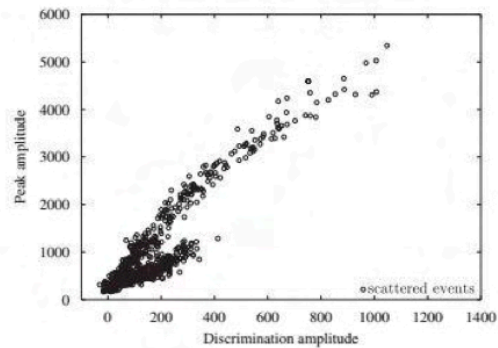
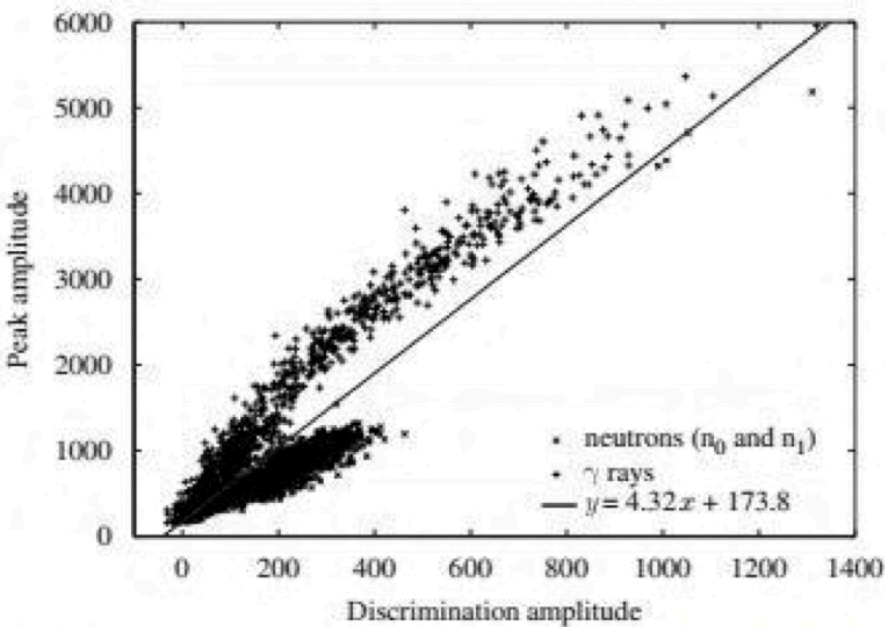
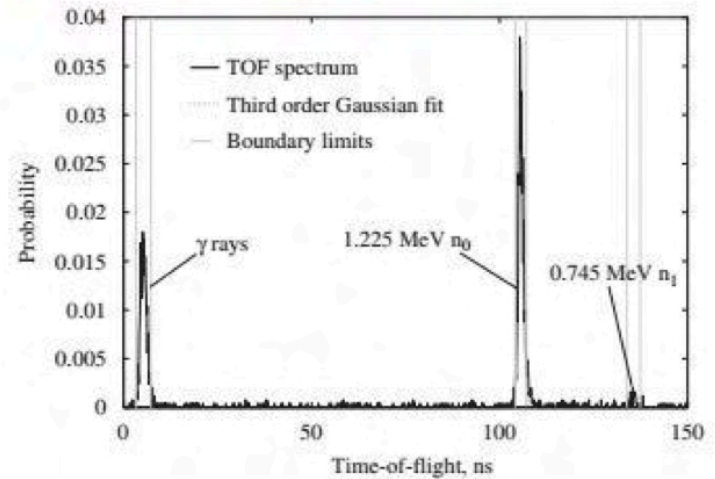
Phoswich made of NaI(Tl) and one of the recently developed IS (LaBr₃:Ce)





Pulse Gradient Analysis (PGA)

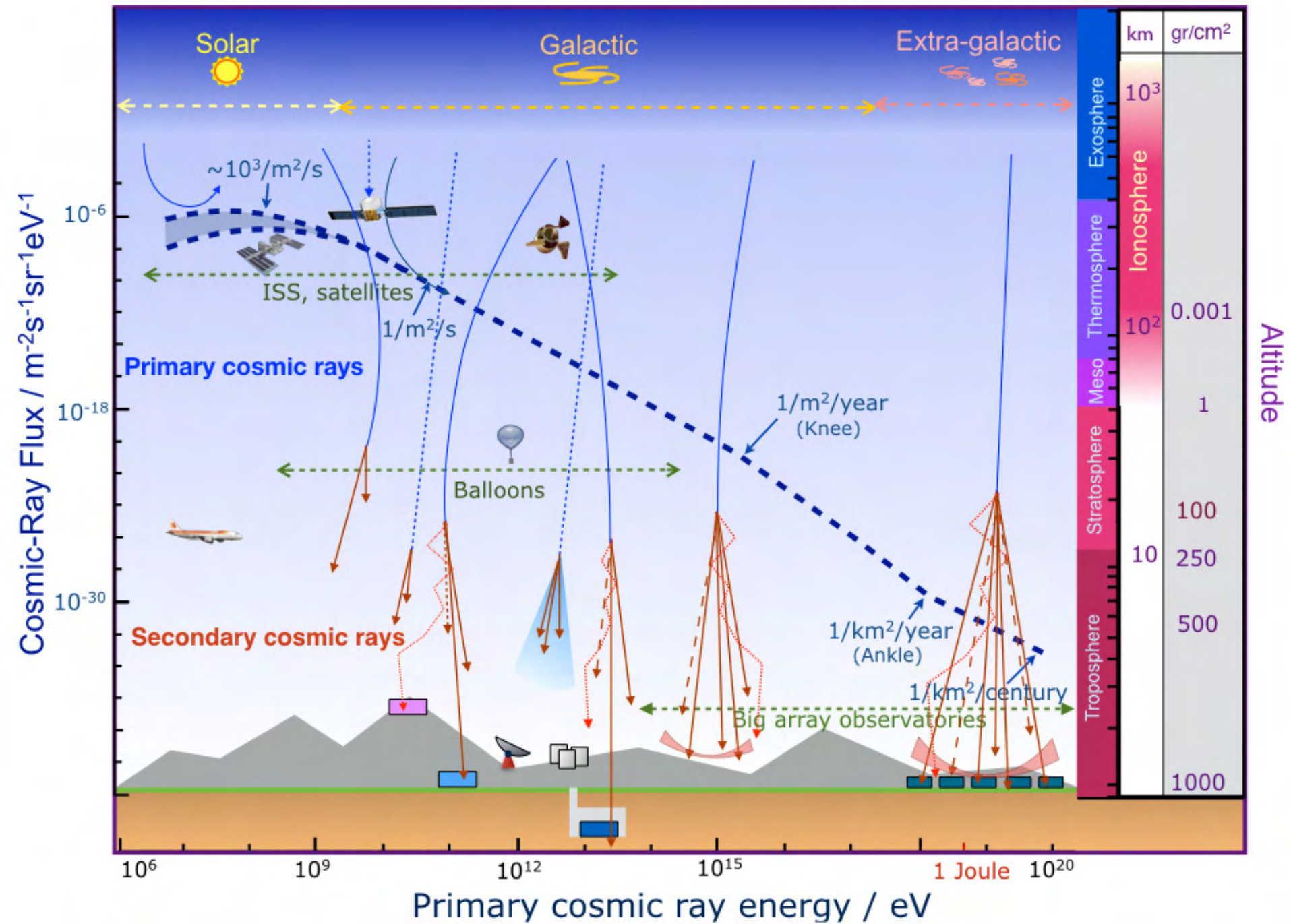
- Comparison of the peak amplitude and amplitude of sample at some later time.
 - Time of Flight (TOF) spectral analysis provides further discrimination.



Some of the latest satellites

RELEC, July 08, 2014 – Dec. 2014, contained 4 phoswich detectors of CsI(Tl)/NaI(Tl) with dimensions of 13 cm diameter, and thicknesses of 0.3 cm for NaI(Tl), 1.7 cm for CsI(Tl) (Panasyuk M. et al. (2017), and 3 CsI(Tl)/BGO phoswich detectors with diameters of 2.0 cm and thicknesses of 0.3 cm for CsI(Tl) and of 1.7 cm for BGO (see Bogomolov et al. (2017).

LOMONOSOV – Apr. 28, 2016 – till pr., 3 phoswich detectors made as CsI(Tl)/NaI(Tl) combination with dimensions of 13 cm diameter, and thicknesses of 0.3 cm for NaI(Tl), 1.7 cm for CsI(Tl) (Svertilov et al. 2018).



Telescope Array in Utah, USA

More than 500 scintillating detectors of 3 m² each, located on a 1.2 km square grid. Additional are three telescope stations on the 30 km triangle. At work since 2007.



ISMART-2018, Minsk (RB), 09-12 October, 2018

The cosmic-ray experiment KASCADE

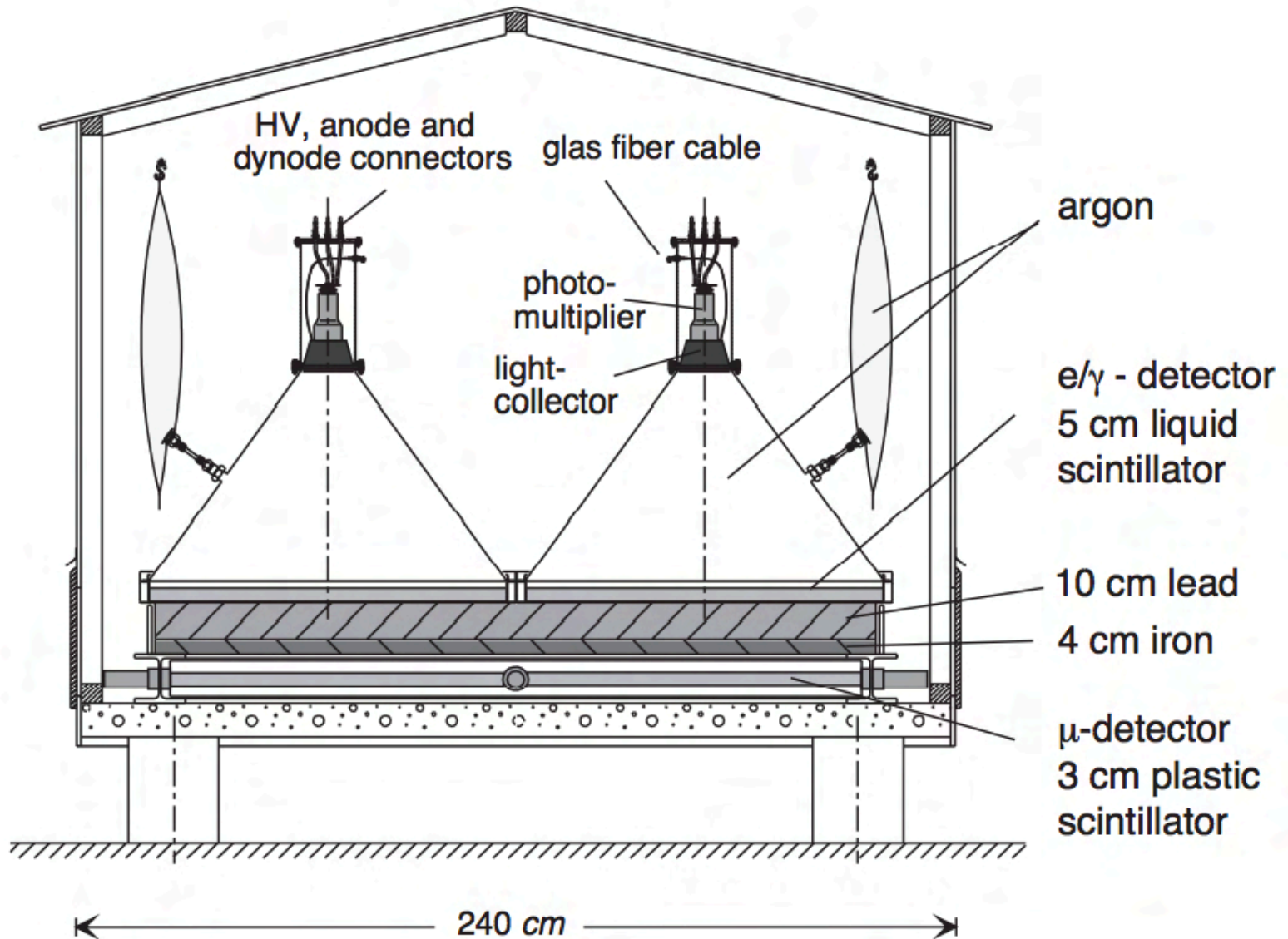


Fig. 4. Sketch of a fully equipped array station with four e/γ detectors on top of a Pb/Fe absorber plate and a segmented muon detector.

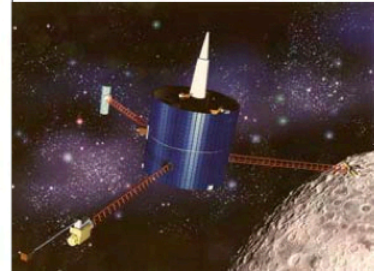
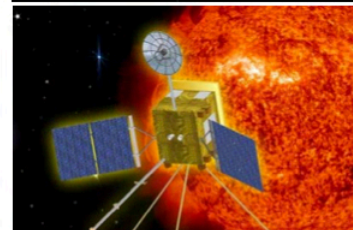
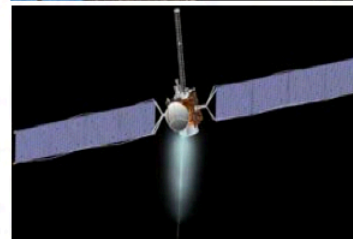
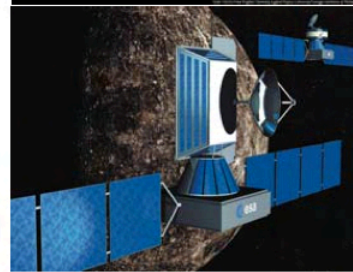
Charged particles and neutral radiation detectors

- Particle spectrometers – in-situ
- Gamma-ray spectrometers (remote sensing, Solar flare and GRB – IPN)
- Neutron detectors (remote sensing and Solar flare)
- S/C radiation monitors

Scintillation Detectors on Planetary Missions

Past missions	GRS	NS	PS
- Phobos	CsI	Stilben,plastic	yes
- Lunar Prospector	BGO/BC454	BC454	
- Near	NaI/BGO		
- Mars Observer	HPGe/BC454	BC454	
- Mars Odyssey	HPGe	BC454,Stilben,plastic	CsI
• Current missions			
- Ulysses	CsI/GRB		Plastic
- Messenger	HPGe/BGO	GS20,BC454	
• Missions in implementation			
- Dawn	CZT/BGO	BGO,BC454, G20	
- Phobos Grunt	LaBr ₃	BC454,Stilben,plastic	
2020 → Solar Orbiter	LaBr ₃	plastic	
2025? → BepiColombo	LaBr ₃		CsI

GRS=gamma-ray spectrometer
 NS=neutron spectrometer
 PS=particle spectrometer



Gamma Rays – Some History (I)

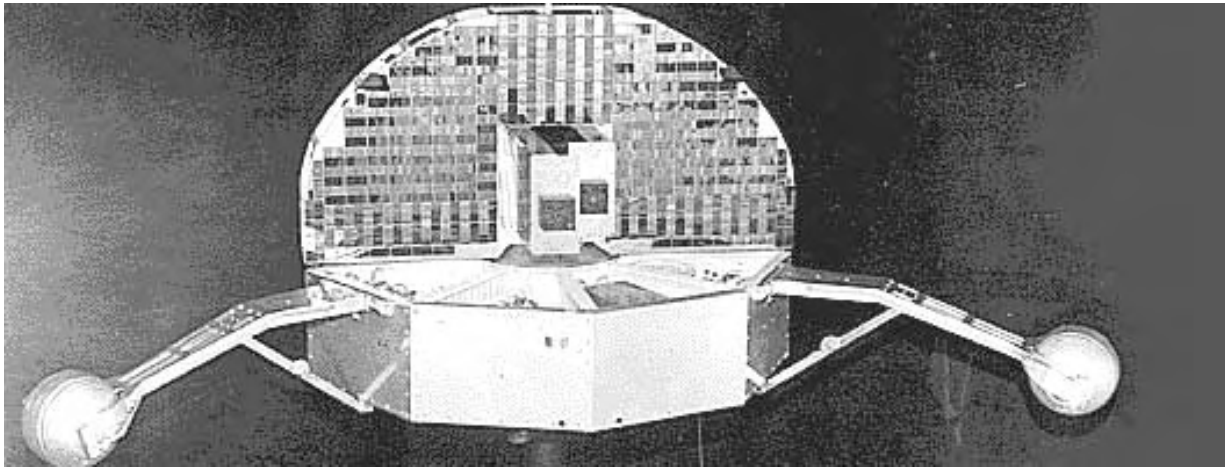
- 1948-1958 – works by Feenberg and Primakoff (1948), Hayakawa and Hutchinson (1952), and Morrison (1958) led scientists to believe that a number of different processes which were occurring in the universe would result in gamma-ray emission
 - Cosmic ray interactions with interstellar gas, supernovae, interactions of energetic electrons with magnetic fields
- 1961 – first gamma-ray telescope, carried into orbit by Explorer XI satellite
 - Picked up < 100 cosmic gamma-ray photons
 - Apparent “uniform gamma-ray background”
- SAS-2 (1972), COS-B (1975-1982) satellites
 - Confirmed earlier findings of gamma-ray background
 - First detailed map of the sky at gamma-ray wavelengths
 - Detection of a few point sources, but poor resolution prevented identification of most of these with individual stars or stellar systems.

Gamma Rays – Some History (II)

- Late 1960's – early 1970's: Vela military satellite series
 - Designed to detect gamma ray flashes from nuclear bomb blasts, recorded gamma-ray bursts from outer space instead
- 1991 – launch of NASA's Compton Gamma Ray Observatory (CGRO)
 - De-orbited in 2001 due to one out of 3 giroscopes failure
- 2002 – launch of the ESA's International Gamma-Ray Astrophysics Laboratory (INTEGRAL). Achievements include:
 - Spectral measurement of gamma-ray sources
 - Detection of GRBs
 - Mapping of the galactic plane in gamma-rays

Orbiting Solar Observatory-1 — OSO-1

OSO-1 — launch: 7 March 1962; data taking till 06 August 1963



Three detector systems were provided as the University of Minnesota Gamma-Ray Telescopes, and together they monitored the intensity and direction properties of gamma-rays between 50 keV and 3 MeV

Orbiting Solar Observatory-1 — OSO-1

The 50-150 keV telescope consisted of NaI(Tl) crystal is 2.54 cm in diameter and 1.27 cm thick. The 31 cm long lead collimator had 0.5 cm thick walls and provided a limited field of view for directional studies.

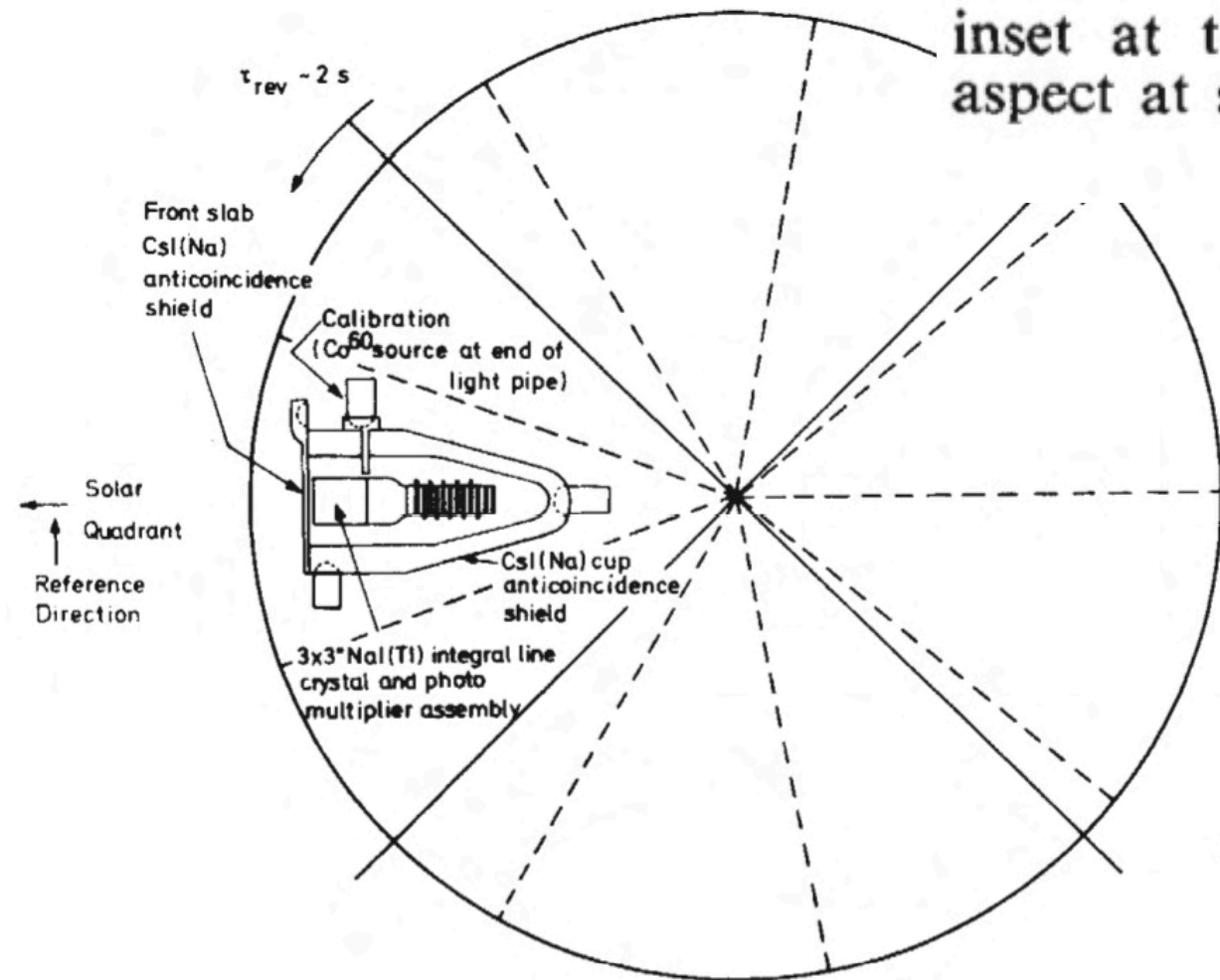
A 5.1 cm diameter by 5.7 cm thick NaI crystal within an NE-102 plastic scintillator of thickness 0.3 cm formed a phoswich detector which had nearly isotropic response. This detector was sensitive to gamma-rays in the 0.33-1 MeV and 1 -3 MeV ranges.

A third NaI crystal with 3.18 cm diameter and 3.18 cm height was placed in conjunction with the phoswich detector and operated in the Compton telescope mode. By proper energy selection of the event in the NaI crystal in coincidence with the phoswich, one gained insight into the incident direction of the gamma-ray. These two telescopes also provided information on the cosmic-ray rates experienced by the Gamma-Ray telescopes.

OSO-7, GRS

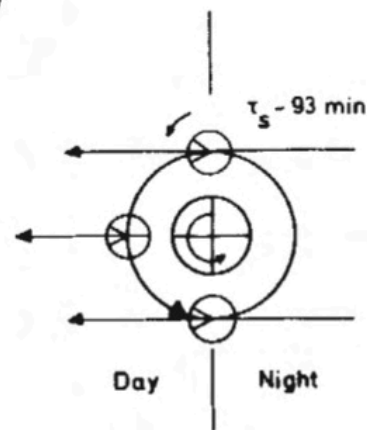
Chupp+1973, Nature,
Solar flare of August 1972

Fig. 1 Schematic drawing of the gamma ray spectrometer, shown with the OSO wheel in the position for viewing the Sun. The solar and background quadrant identifications are also shown. The small inset at the right shows satellite aspect at sunrise and at noon and at sunset.



Background
Quadrant

GRM was 3x3 inch
NaI(Tl) inside of
anticoinc. shield
made of CsI(Na)



HEAO-3, GRS

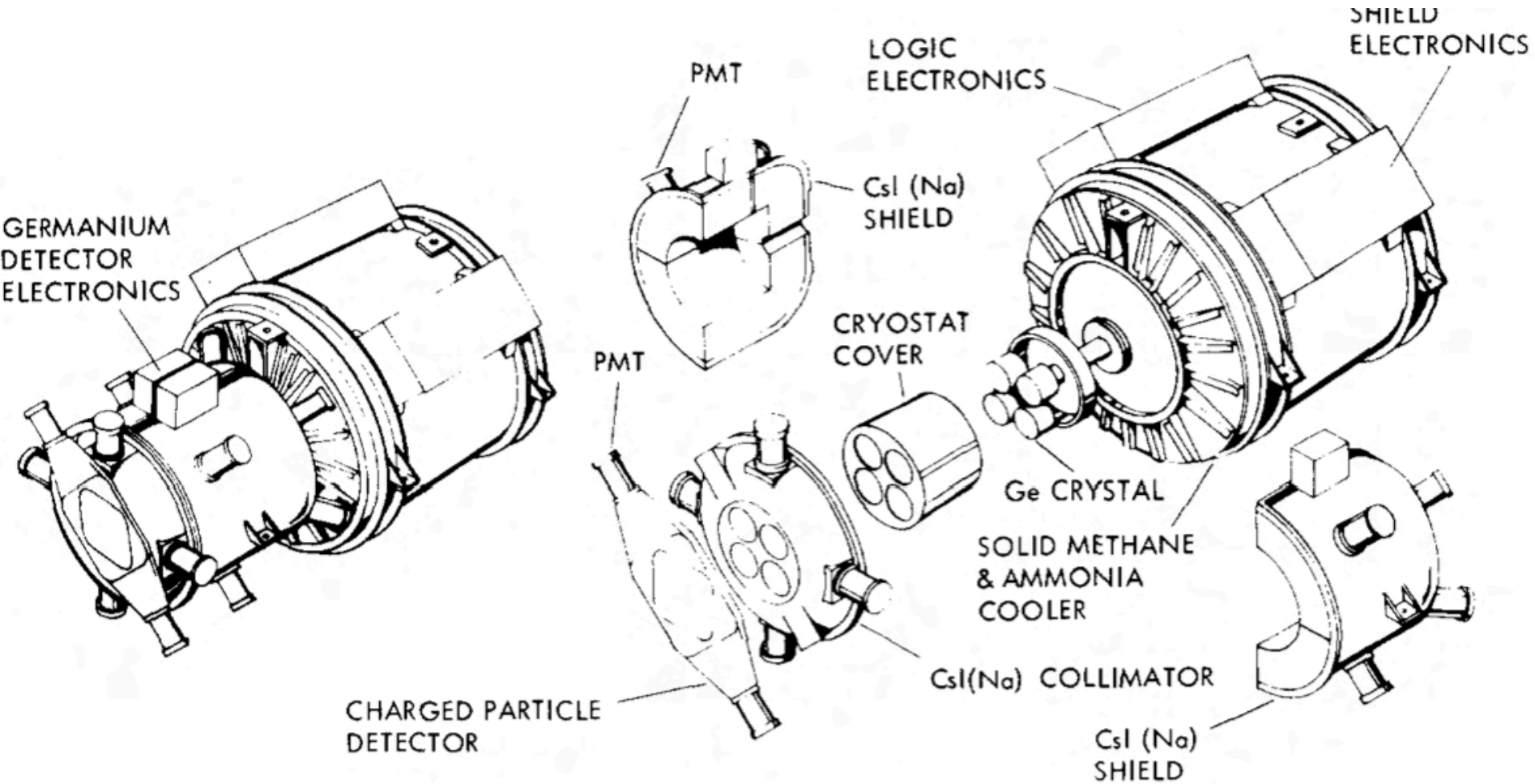


Fig. 1. An exploded view of the experiment.

HEAO-3, GRS

tude of 500 km and an inclination of 43.6° . On board is the GRS experiment which consists basically of a cluster of four cooled high purity germanium detectors surrounded by an active anti-coincidence shield of CsI(Na) (fig. 1). The instrument itself is roughly cylindrical in shape with a diameter of 0.8 m and a length of 1.2 m. It weighs approximately 235 kg and consumes an average power of 25 W.

A hole in the collimator above each germanium detector gives the instrument a field of view of about 30° fwhm. The view axis of the instrument points at right angles to the spacecraft spin axis, which always points toward the sun, so that the GRS experiment performs a complete sky survey every six months. The observatory spins with a period of approximately 20 min.

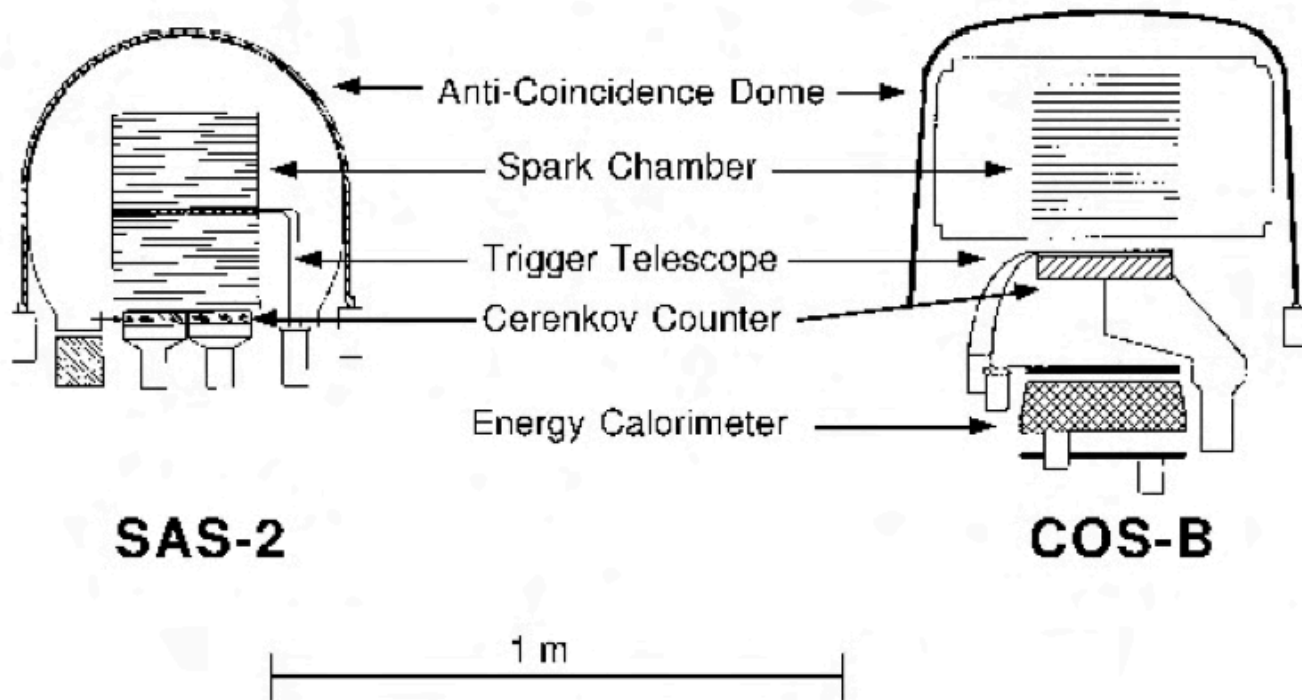
SAS-II

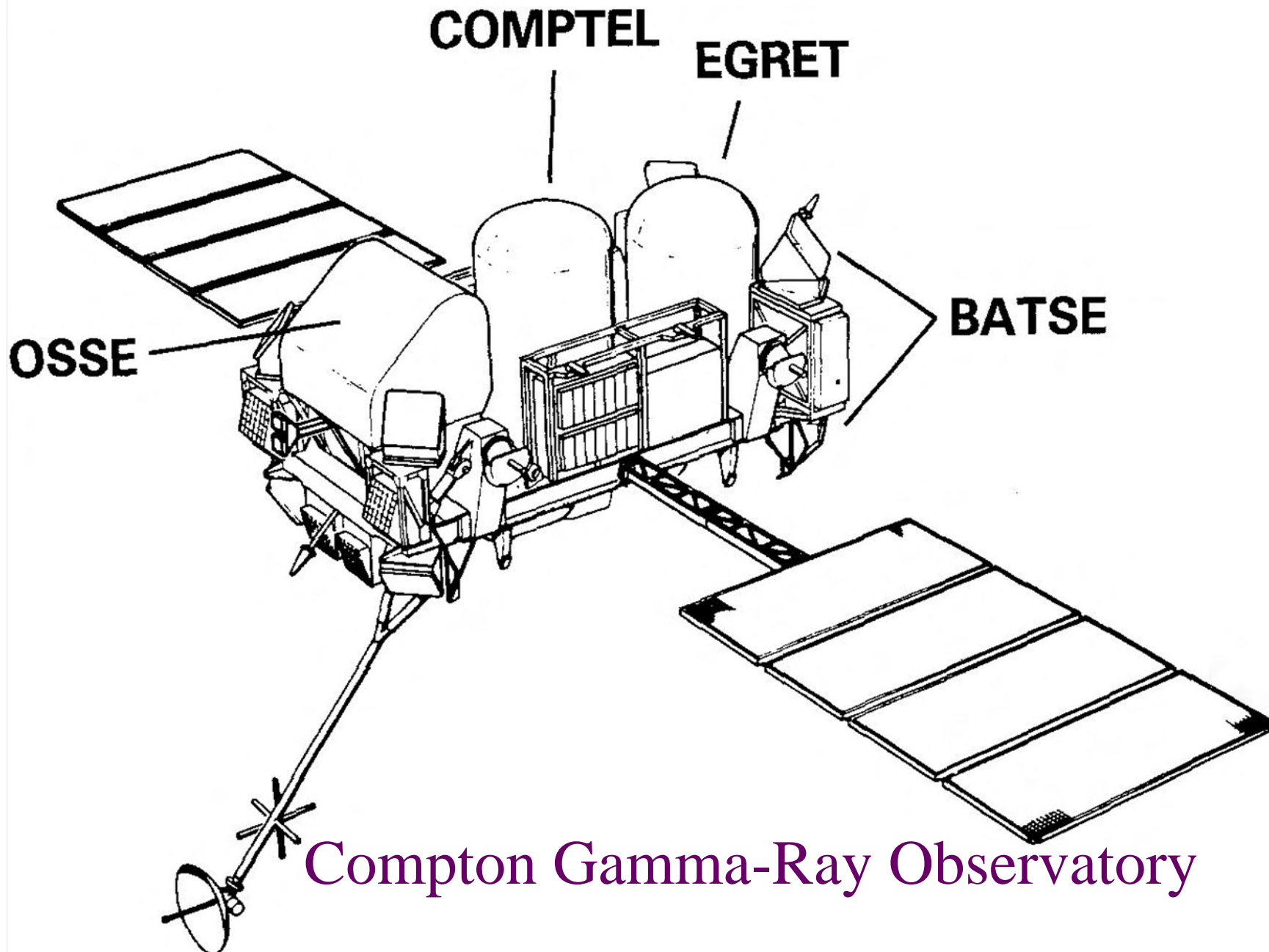
PI-Carl Fichtel

Nov 20, 1972-June 08

1973; mass – 166 kg

Gamma Ray Telescopes





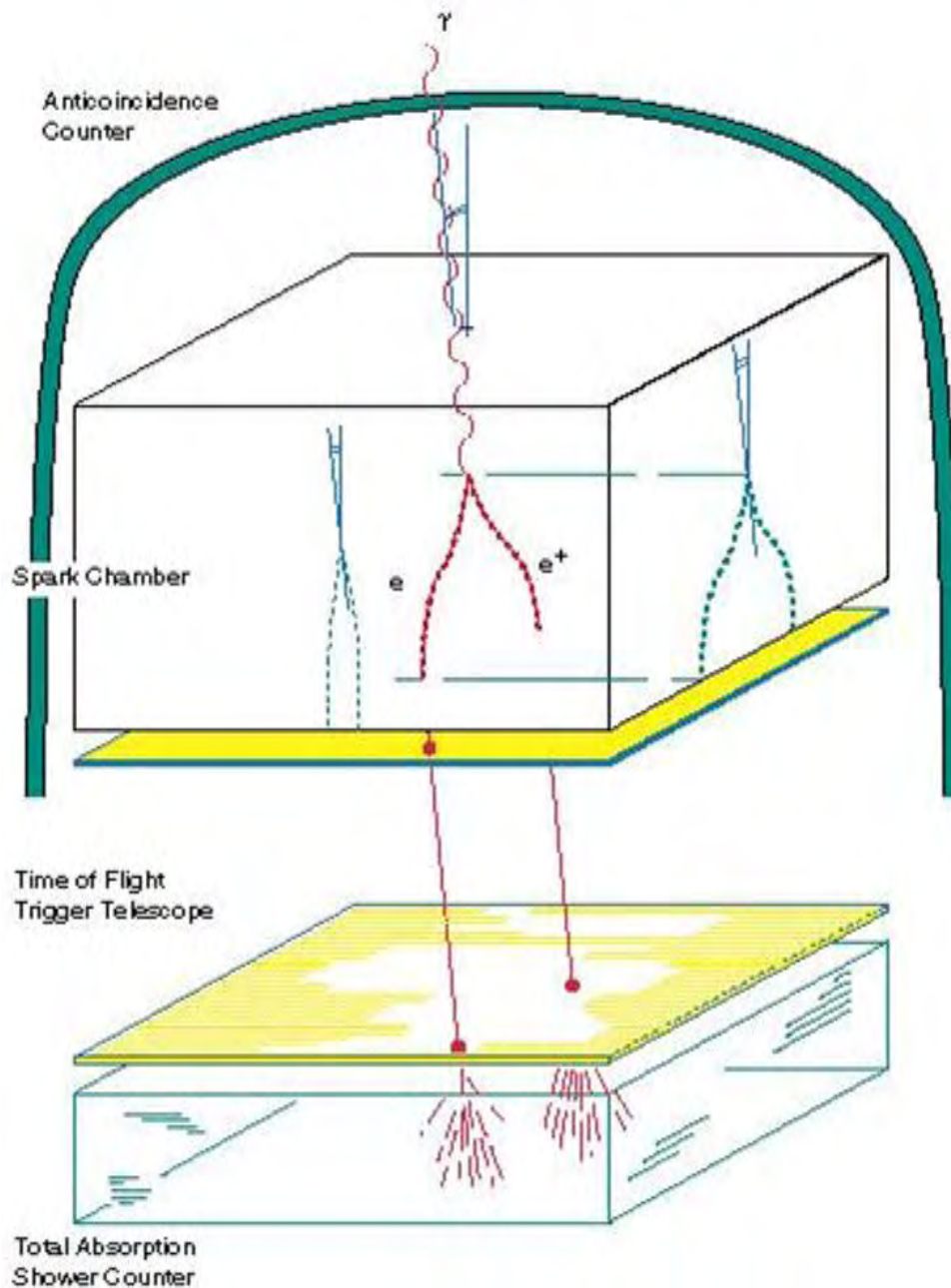
ISMART-2018, Minsk (RB), 09-12 October, 2018

EGRET

PI-Carl Fichtel

April, 1991-June 2001

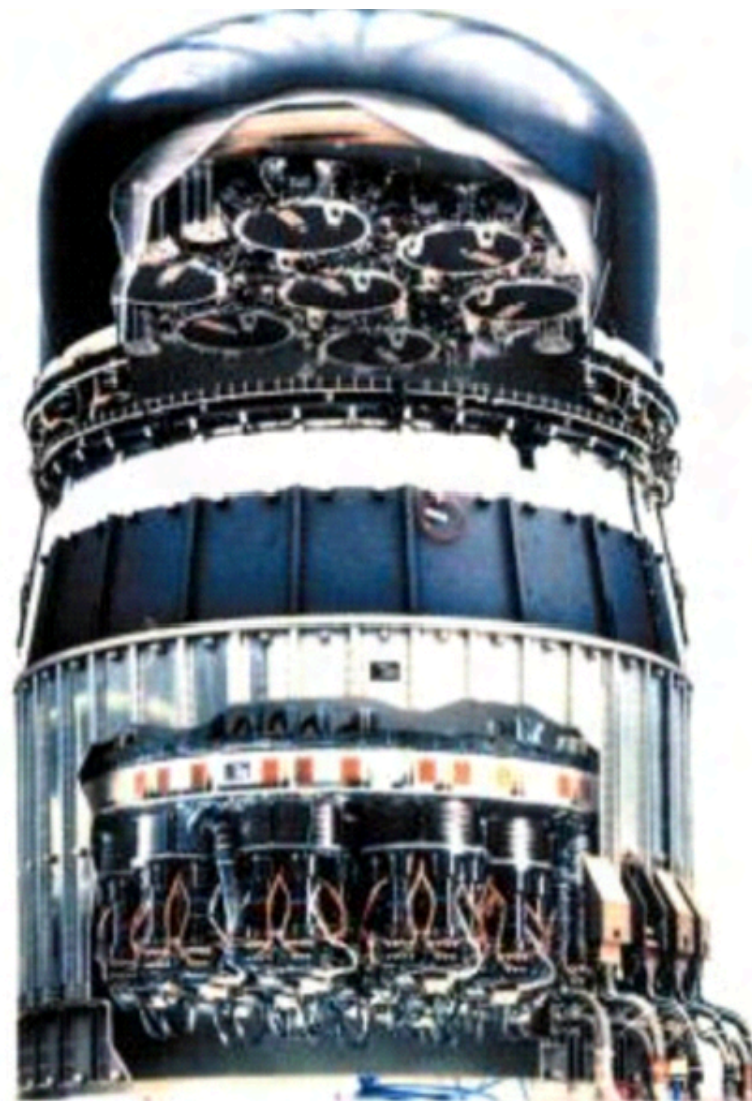
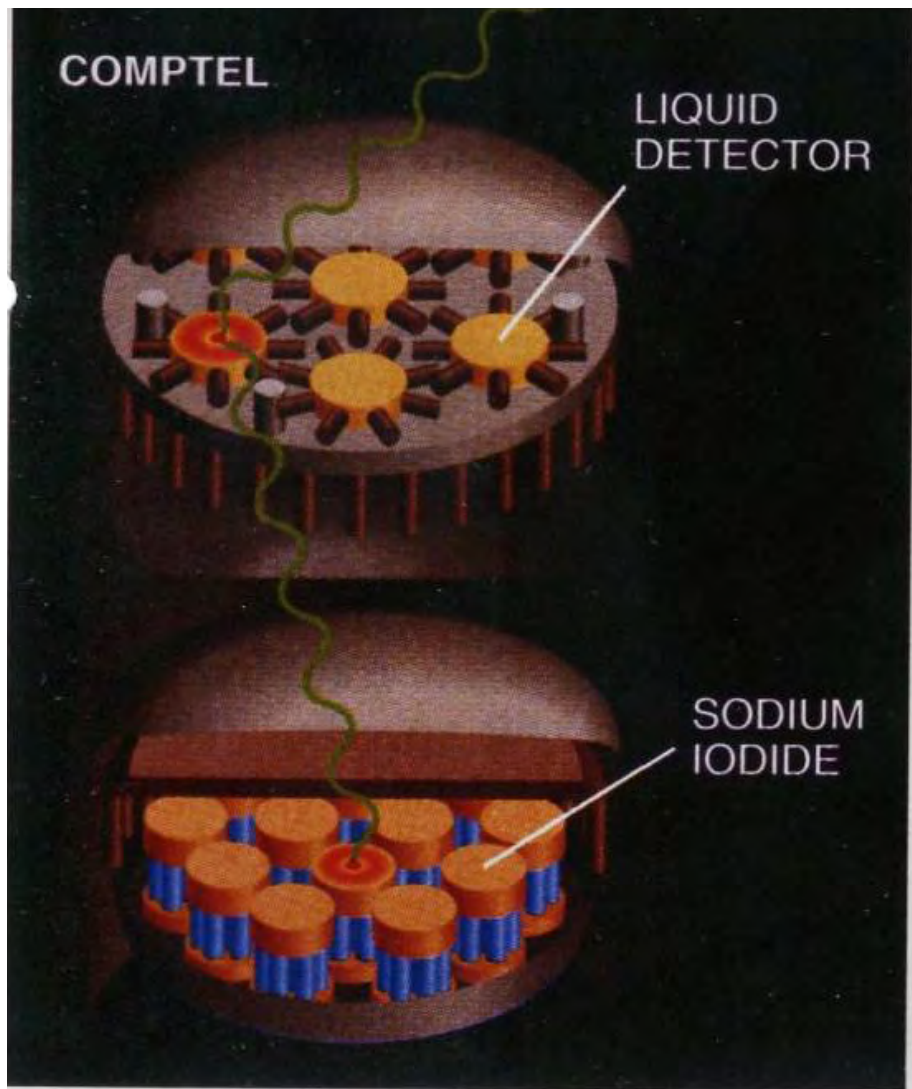
Mass – 1830 kg



EGRET physical characteristics

Mass:	1830 kg
Length/Diameter:	2.25 m/1.65 m
Power (incl. heater):	190 W
Data:	6859 bits s ⁻¹

CGRO-COMPTEL



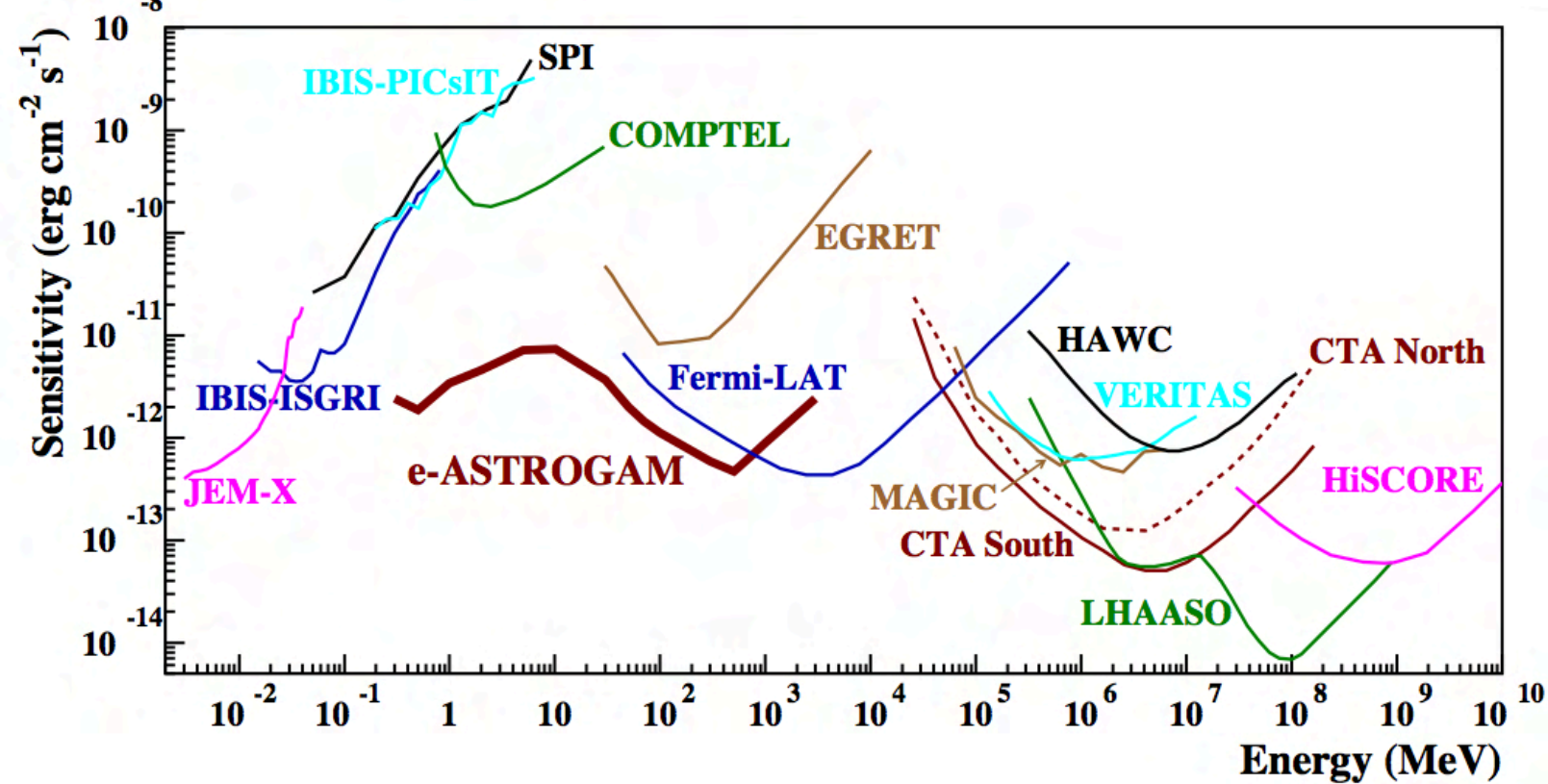


Fig. 1: Point source continuum sensitivity of different X- and γ -ray instruments. The curves for *INTEGRAL*/JEM-X, IBIS (ISGRI and PICsIT), and SPI are for an effective observation time $T_{\text{obs}} = 1$ Ms. The COMPTEL and EGRET sensitivities are given for the typical observation time accumulated during the ~ 9 years of the *CGRO* mission (see Fig. 1 in [97]). The *Fermi*/LAT sensitivity is for a high Galactic latitude source in 10 years of satellite observation in survey mode. For MAGIC, VERITAS (sensitivity of H.E.S.S. is similar), and CTA, the sensitivities are given for $T_{\text{obs}} = 50$ hours. For HAWC $T_{\text{obs}} = 5$ yr, for LHAASO $T_{\text{obs}} = 1$ yr, and for HiSCORE $T_{\text{obs}} = 1000$ h. The e-ASTROGAM sensitivity is for an effective exposure of 1 year for a source at high Galactic latitude.

eASTROGAM

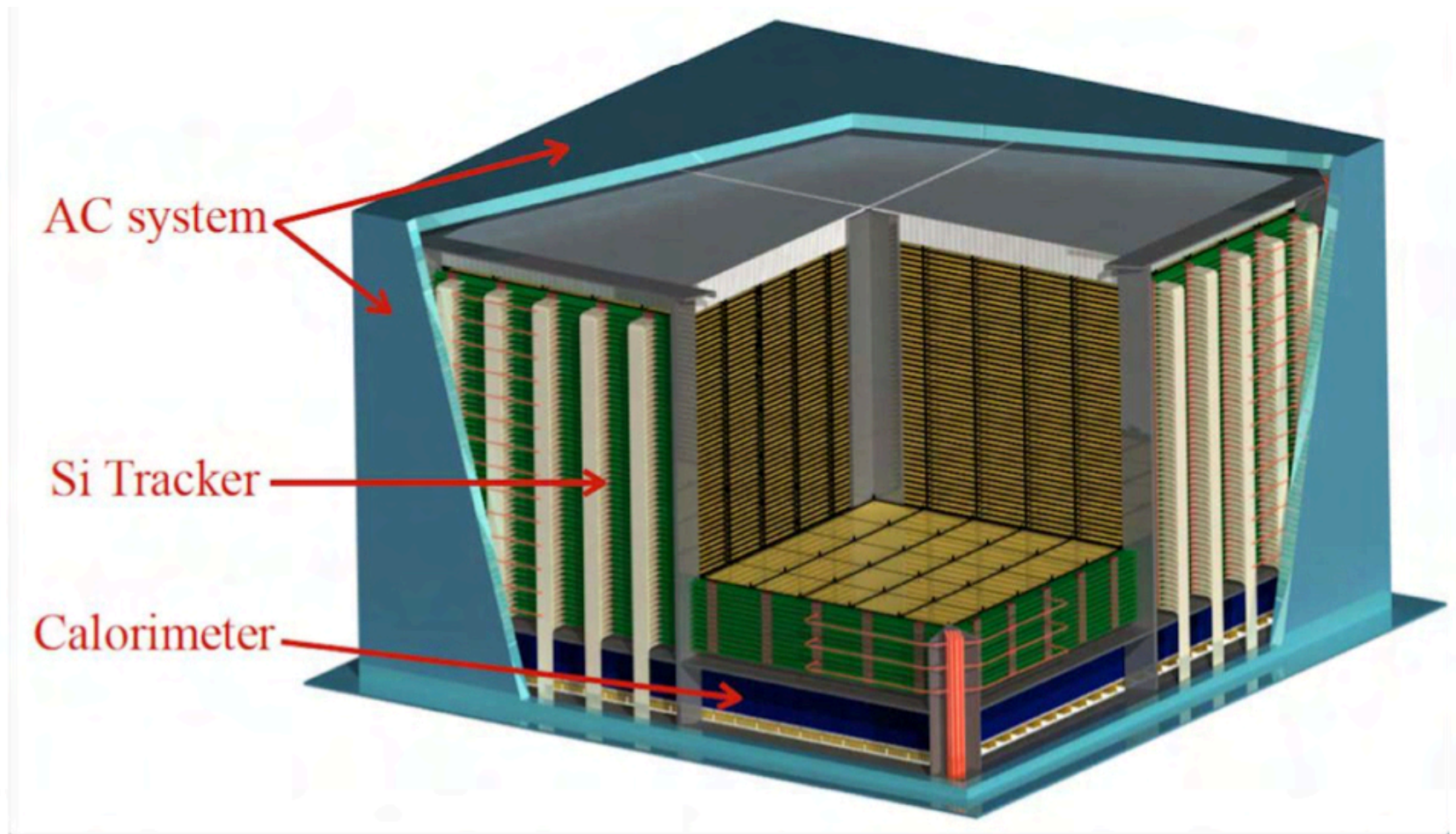
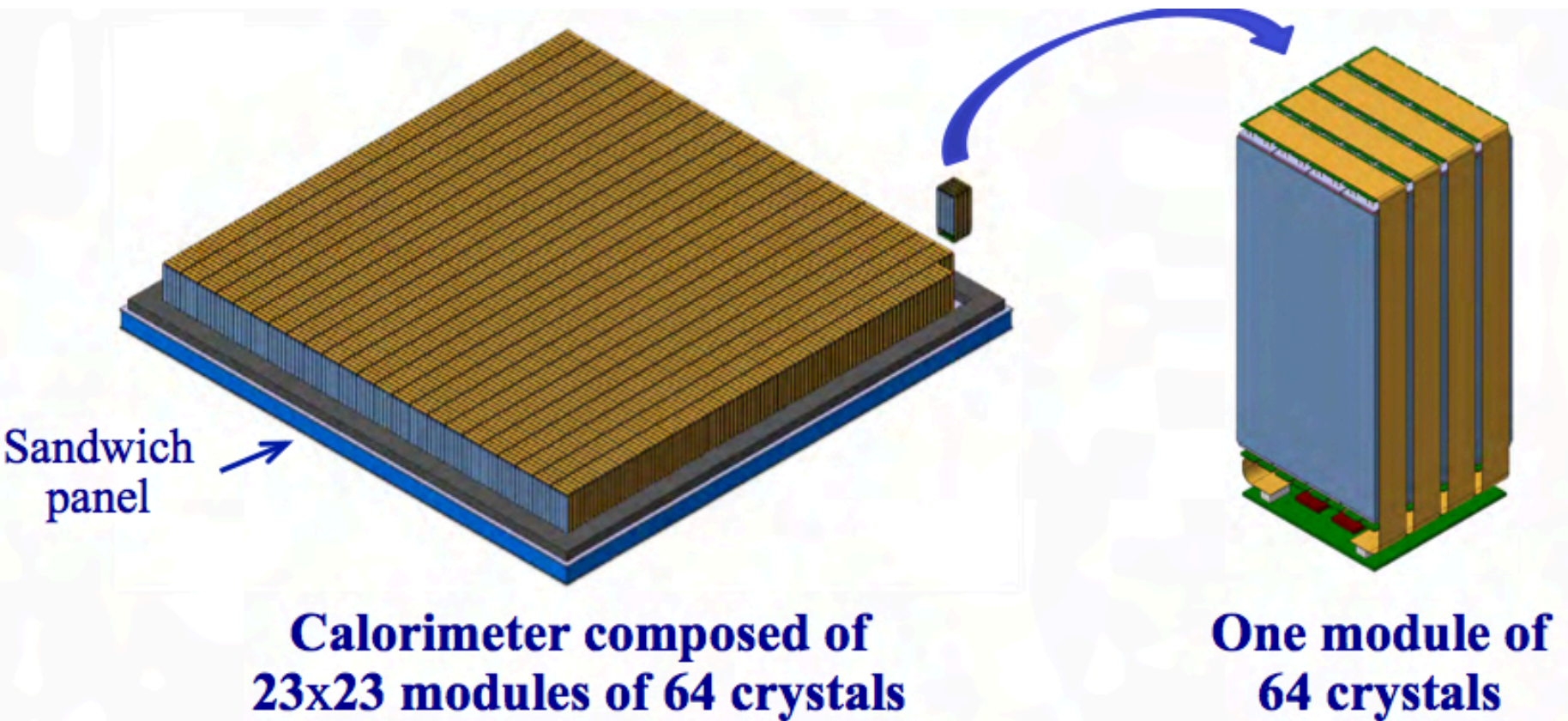


Fig. 12: Overview of the e-ASTROGAM payload showing the silicon Tracker, the Calorimeter and the Anticoincidence system.

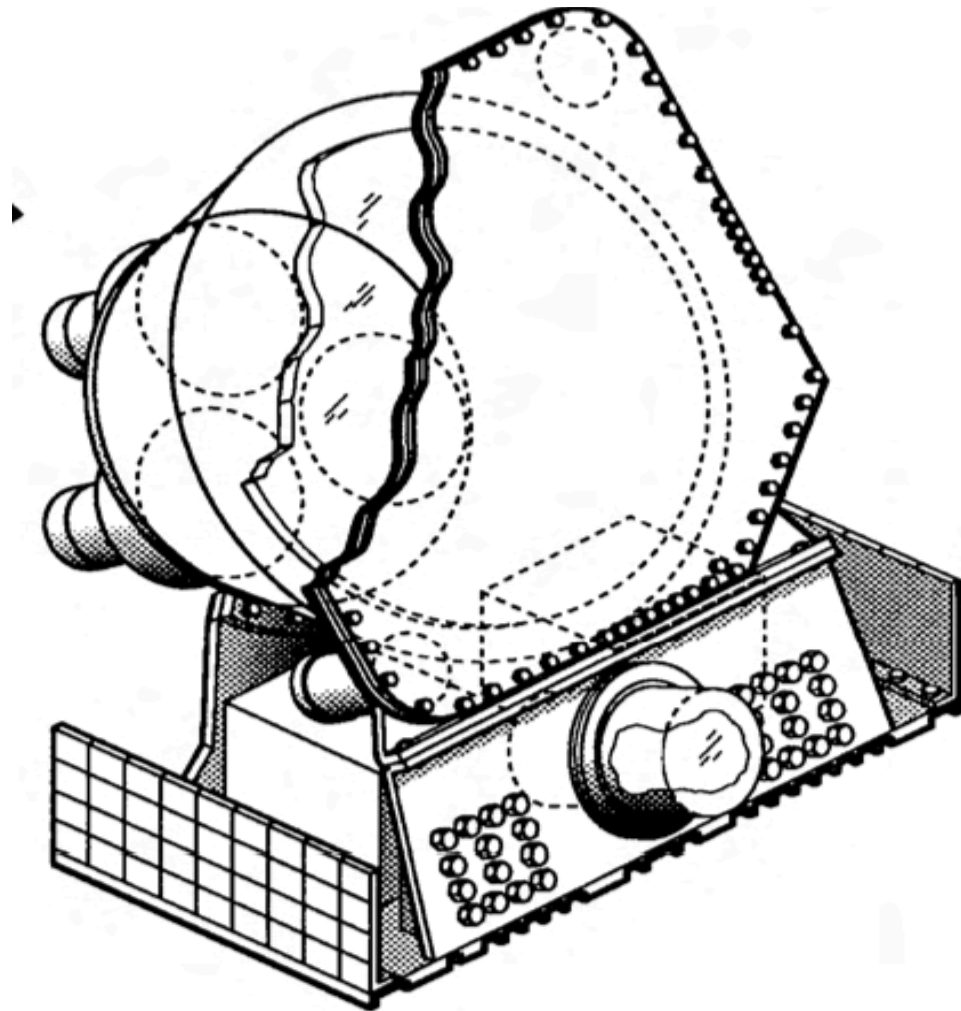
eASTROGAM, calorimeter

CeBr₃ – CsI(Tl) ???



Overview of the Calorimeter and of one of its 529 ($= 23 \times 23$) comprising 64 CsI(Tl) crystals.

BATSE - an answer to GRB quest



Each of 8 modules is of 50.8 cm diameter and 1.27 cm thick.

ISMART-2018, Minsk (RB), 09-12 October, 2018



Vela-project

Vela sats series began with the launch of Vela 1/2 on October 17, 1963, a flight also marking the maiden launch of the Atlas-Agena SLV-3 vehicle. The second pair of satellites launched on July 17, 1964, and the third on July 20, 1965.

The original Vela satellites were equipped with 12 external X-ray detectors and 18 internal neutron and gamma-ray detectors. They were equipped with solar panels generating 90 watts.

Detectors of Vela-project

The scintillation X-ray detector (XC) aboard Vela 5A and its twin Vela 5B consisted of two 1 mm thick NaI(Tl) crystals mounted on photomultiplier tubes and covered by a 0.13 mm thick beryllium window. Electronic thresholds provided two energy channels, 3–12 keV and 6–12 keV.

In front of each crystal was a slat collimator providing a full width at half maximum (FWHM) aperture of $\sim 6.1 \times 6.1$ degrees. The effective detector area was $\sim 26 \text{ cm}^2$. The detectors scanned a great circle every 60 seconds.

Sensitivity to celestial sources was severely limited by the high intrinsic detector background, equivalent to about 80% of the signal from the Crab Nebula, one of the brightest sources in the sky at these energies.

Vela-project and GRBs

On July 2, 1967, at 14:19 UTC, the Vela 4 and Vela 3 satellites detected a flash of gamma radiation unlike any known nuclear weapons signature. Uncertain what had happened but not considering the matter particularly urgent, the team at the Los Alamos National Laboratory, led by Ray Klebesadel, filed the data away for investigation. As additional Vela satellites were launched with better instruments, the Los Alamos team continued to find inexplicable gamma-ray bursts in their data. By analyzing the different arrival times of the bursts as detected by different satellites, the team was able to determine rough estimates for the sky positions of sixteen bursts and definitively rule out a terrestrial or solar origin. The discovery was declassified and published in 1973 an article entitled "Observations of Gamma-Ray Bursts of Cosmic Origin". This alerted the astronomical community to the existence of gamma-ray bursts (GRBs), now recognised as the most violent events in the universe.

World space program

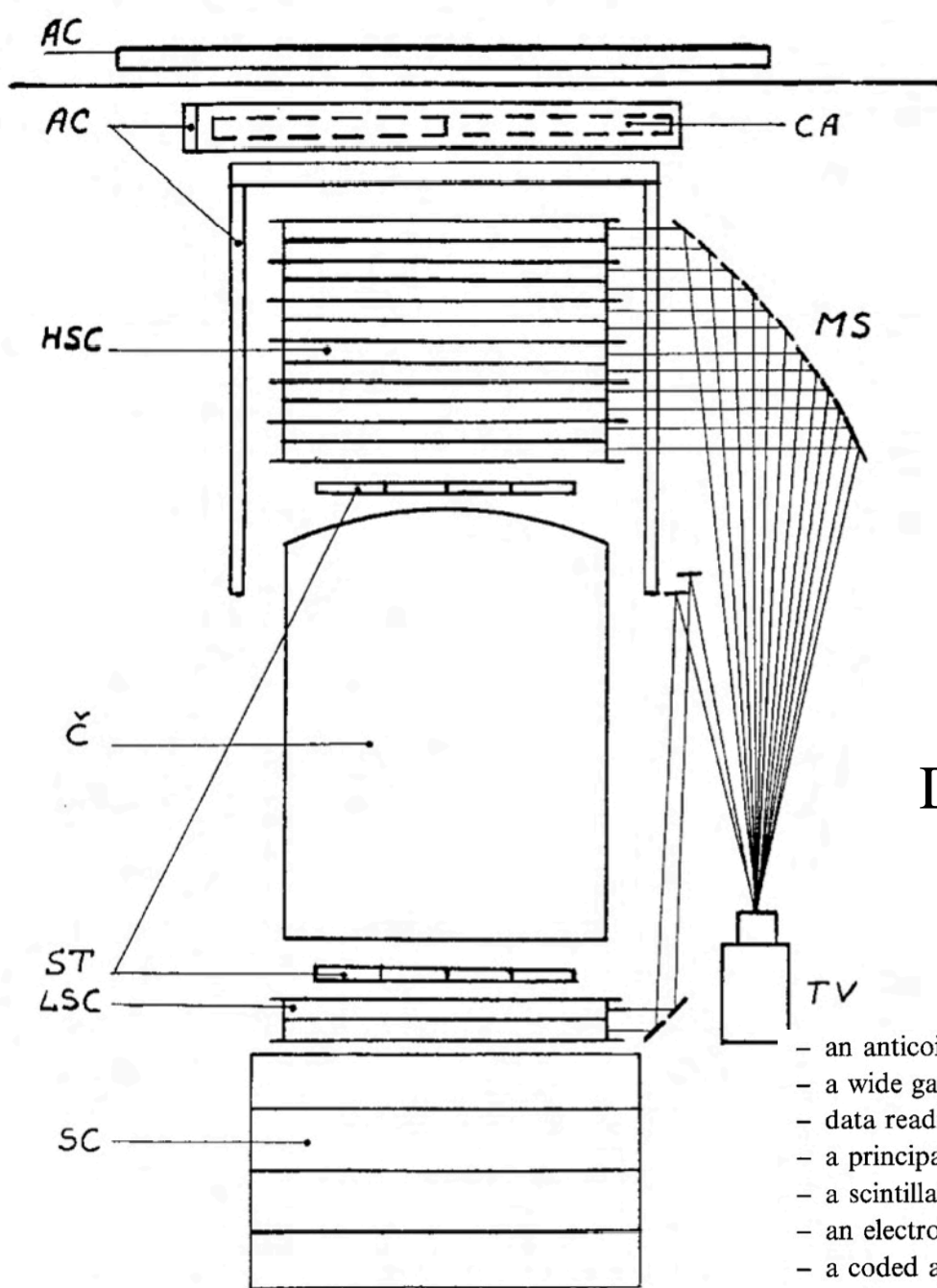
All together more than 120 experiments dedicated to space exploration of X-ray and gamma-ray sky were (are) executed until present.

Majority of those were mostly USA, and/or international orbital solar observatories, high-energy astrophysical observatories and similar.

Among scintillating detectors NaI(Tl), CsI(Tl) and CsI(Na) are the most popular.

Planetary automatic stations are also numerous.

USSR and RF performed > 30 experiments in X-ray and gamma-ray, program.



Gamma-1

11 July 1990-01 Jan. 1992
 PI-Kirillov-Ugryumov V.G.

Height of >3 meters
 Total weight 1650 kg
 Power consumption 300W

Detected solar flare of June 1991
 $20 \text{ keV} < E_{x,g} < 6 \text{ GeV}$

- an anticoincidence counter system (AC);
- a wide gap spark chamber system (HSC, LSC);
- data reading from spark chambers (mirror and TV systems) (MS, TV);
- a principal starting telescope (scintillation and Čerenkov gas counters) (ST, Č);
- a scintillation calorimeter (SC);
- an electronic control and telemetering formation system;
- a coded aperture system (CA);
- a star sensor.

Fig. 1. A schematic diagram of the 'Gamma-1' telescope.

Fermi-LAT

Launched June, 2008
PI-Peter Mikelson
USA, Germany,
France, Italy, Japan,
Spain, Sweden

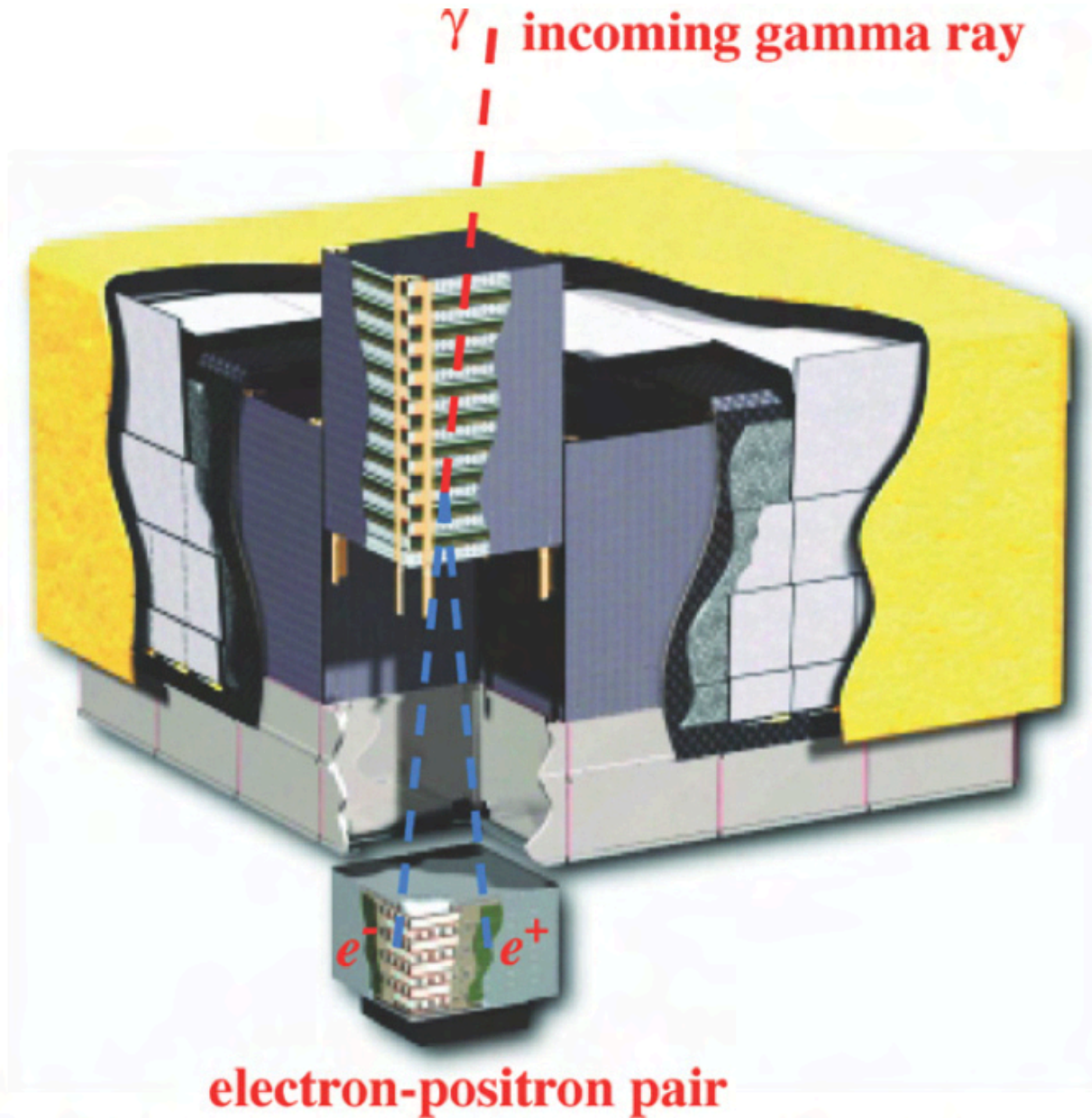


Figure 1. Schematic diagram of the LAT. The telescope's dimensions are $1.8 \text{ m} \times 1.8 \text{ m} \times 0.72 \text{ m}$. The power required and the mass are 650 W and 2789 kg , respectively.

LAT-calorimeter

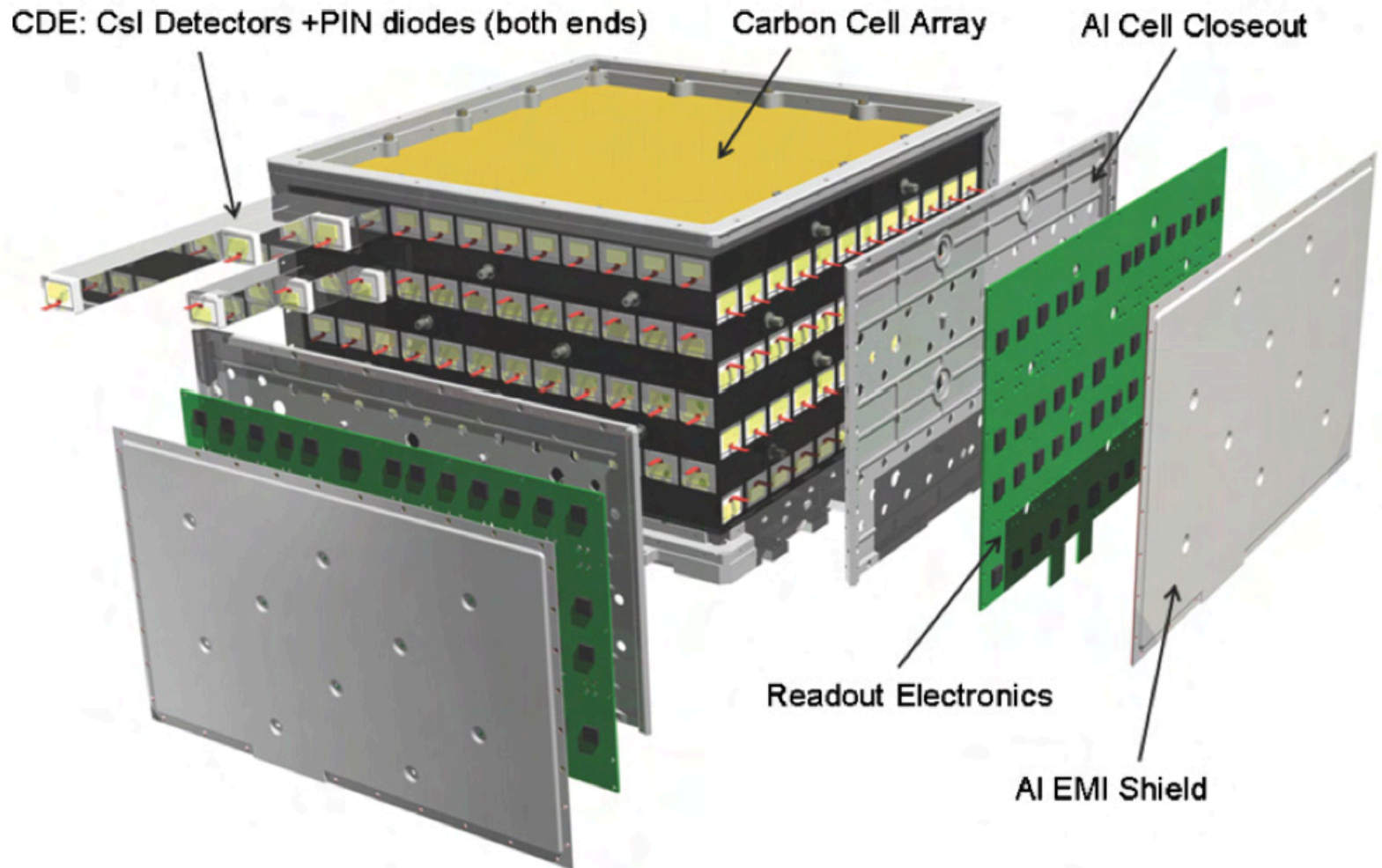
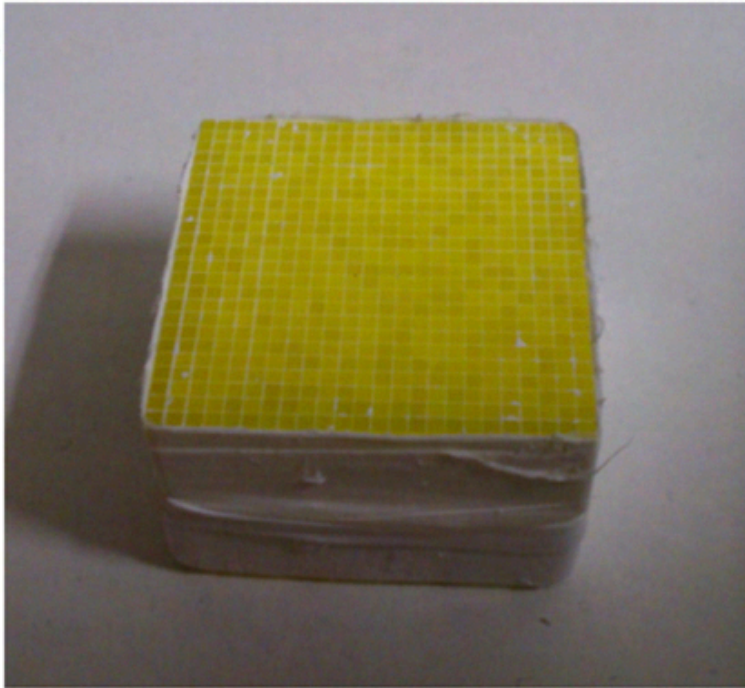


Figure 6. LAT calorimeter module. The 96 CsI(Tl) scintillator crystal detector elements are arranged in eight layers, with the orientation of the crystals in adjacent layers rotated by 90° . The total calorimeter depth (at normal incidence) is 8.6 radiation lengths.

Pixellated detectors

Ce doped $\text{Gd}_3\text{Ga}_3\text{Al}_2\text{O}_{12}$ (GFAG) and Ce doped $\text{Gd}_3\text{Al}_2\text{Ga}_3\text{O}_{12}$ (GAGG) are newly developed scintillator for radiation detectors. GAGG

A



B

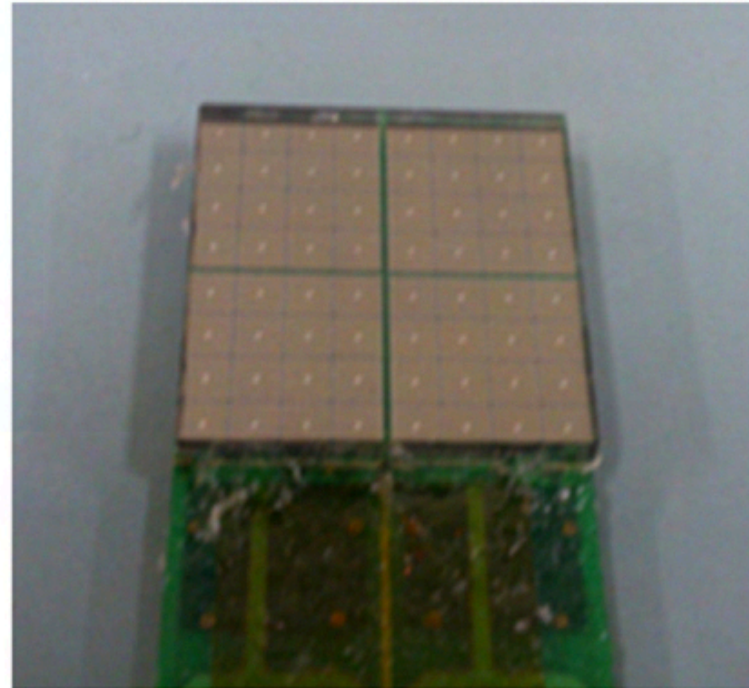


Fig. 2. Photographs of phosphor scintillator block (A), Si-PM array (B) :

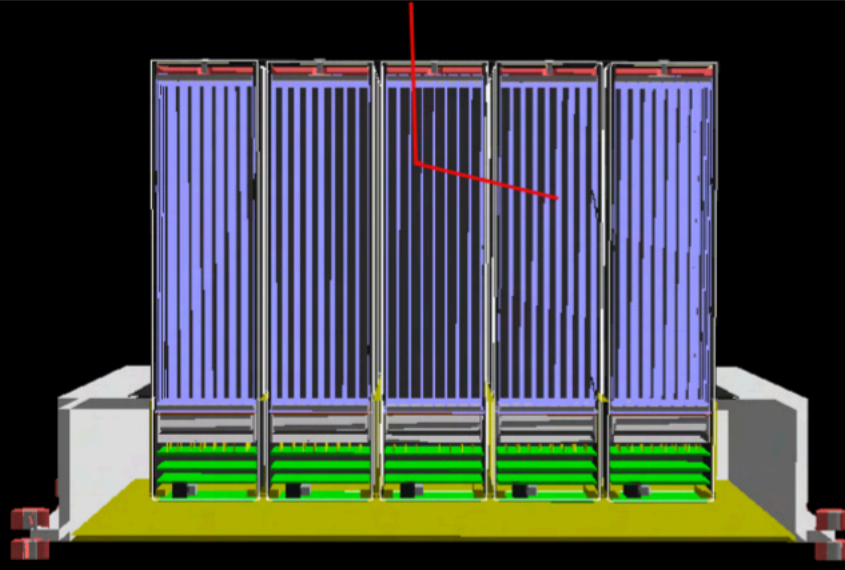
POLAR

Switzerland, China, Poland

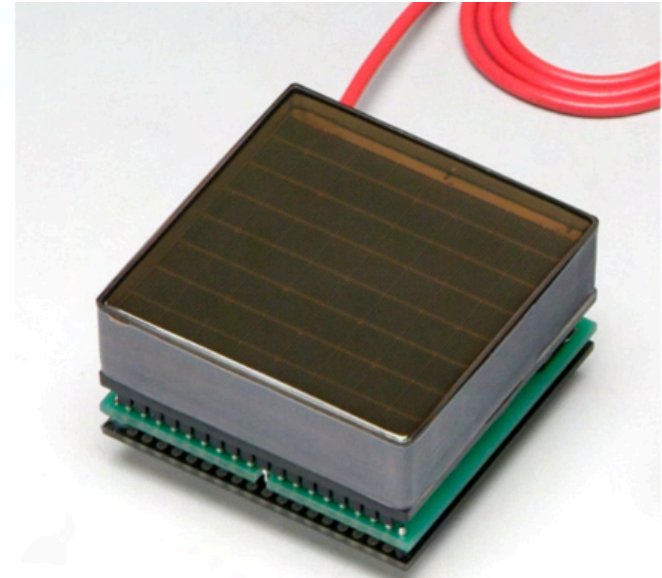
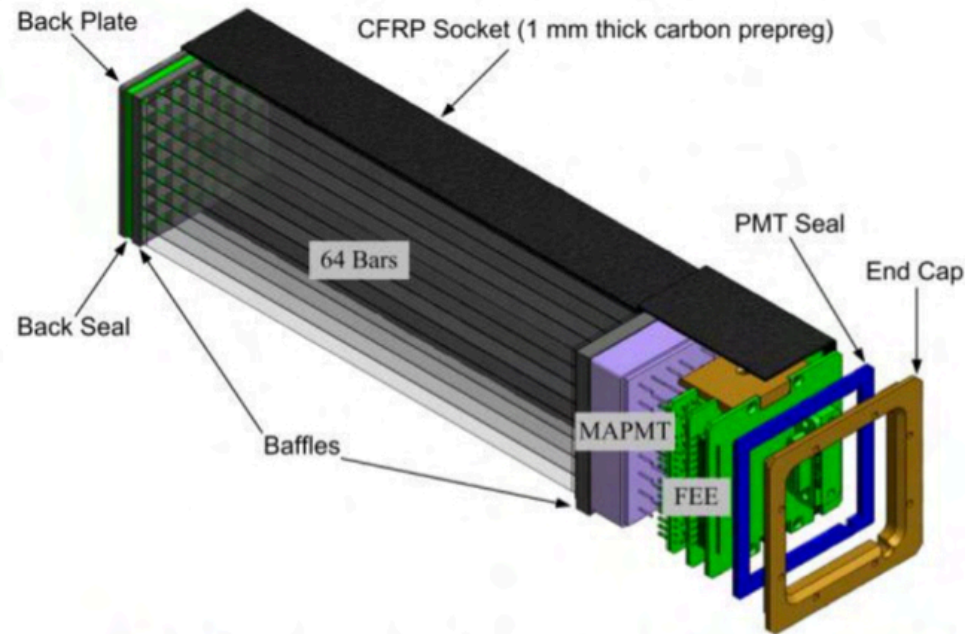
PI- Nicolas Produit

Launched Sept.15, 2016

Oon-board TG-2 mission

- 
- Relatively large effective area
 - Small pixels allows for high precision scattering angle measurements
 - Uniform effective area gives us a large Field of View
 - We see half of the sky and perform polarimetry for sources within 1/3rd of the sky
 - Full description of the instrument recently published: N. Produit et al. [arXiv:1709.07191](https://arxiv.org/abs/1709.07191)

POLAR



from: www.hamamatsu.com

- Each group of 64 scintillators is read-out using a single MAPMT
- MAPMT is H8500 from Hamamatsu
- Allows for the read-out many channels with a sufficient gain to measure low energy depositions
- Optical cross-talk to neighbouring channels is an issue but can be fixed in analysis
- Cross talk reduced by shaping of scintillators

One module consists of 64 bars made of a 176 mm long plastic cuboid of EJ248M. POLAR has 25 modules.

PoGOLite

PI-Mark Pearce
KTH, Sweden

Based on the use of
phoswich detector cells

Phoswich consists
of three scintillators
a 60 cm long plastic
tube of EJ240, a 20
cm long EJ204 rod,
and a 4 cm long BGO

Each of 61 PDC has
a hexagon shape

All PDCs are surro-
unded by SAS made
of BGO

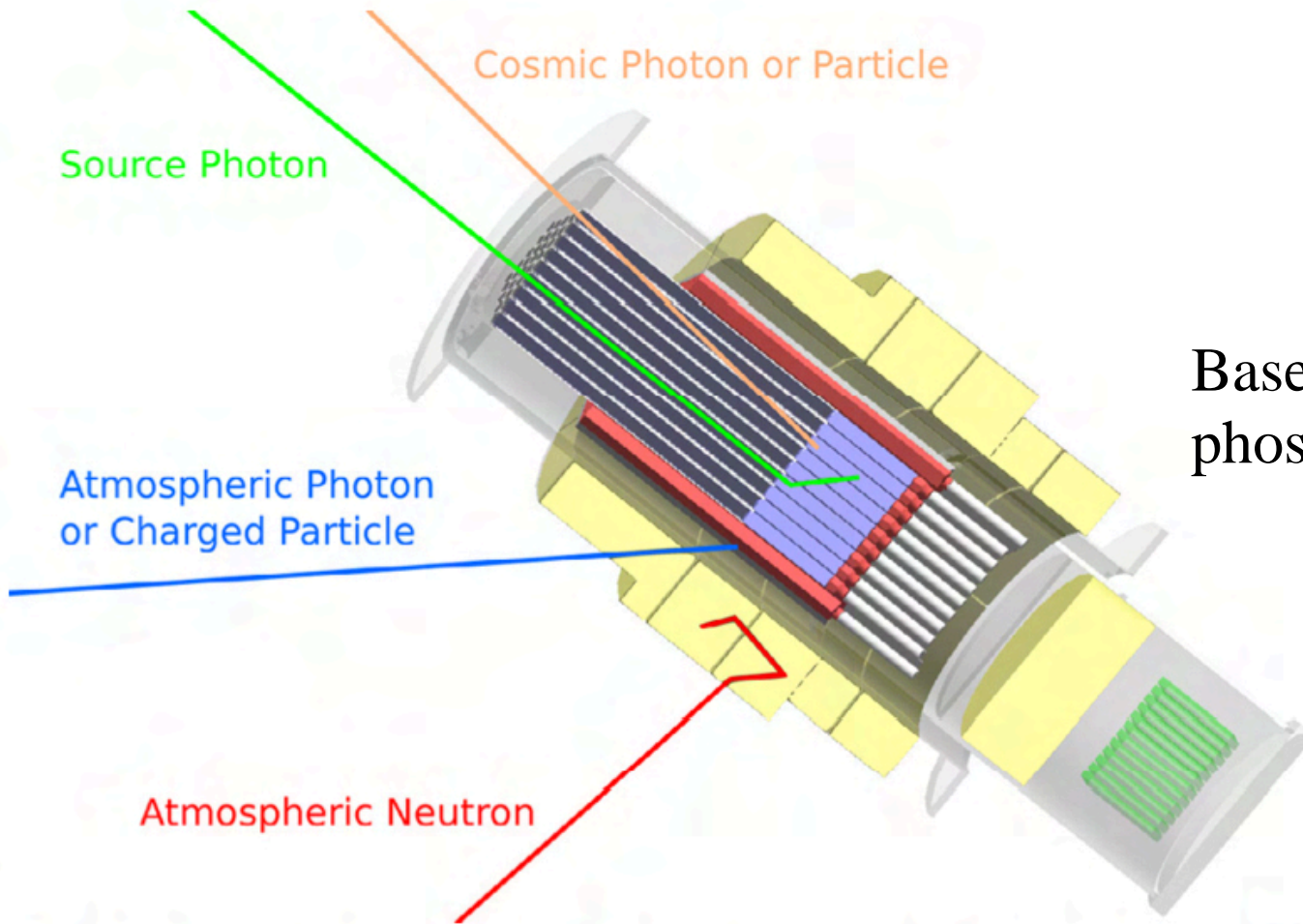


Fig. 2. A schematic cross-section of the PoGOLite Pathfinder instrument. The scintillator scattering target is shown in blue, while the hollow collimating scintillators are shown in black and the BGO units in red. The scintillators are read out by photomultipliers (white). The polarimeter is housed in a pressure vessel (grey), which in turn is surrounded by a polyethylene neutron shield (yellow). The data acquisition electronics (green) are placed at the bottom of the instrument. Possible interactions of photons and particles with the detector elements are indicated. The telescope measures about 1.5 m from top to bottom and its aperture is about 30 cm wide. (For interpretation of the references to colour in this figure legend, the reader is referred to the web version

2D diagram of PoGO Lite signals

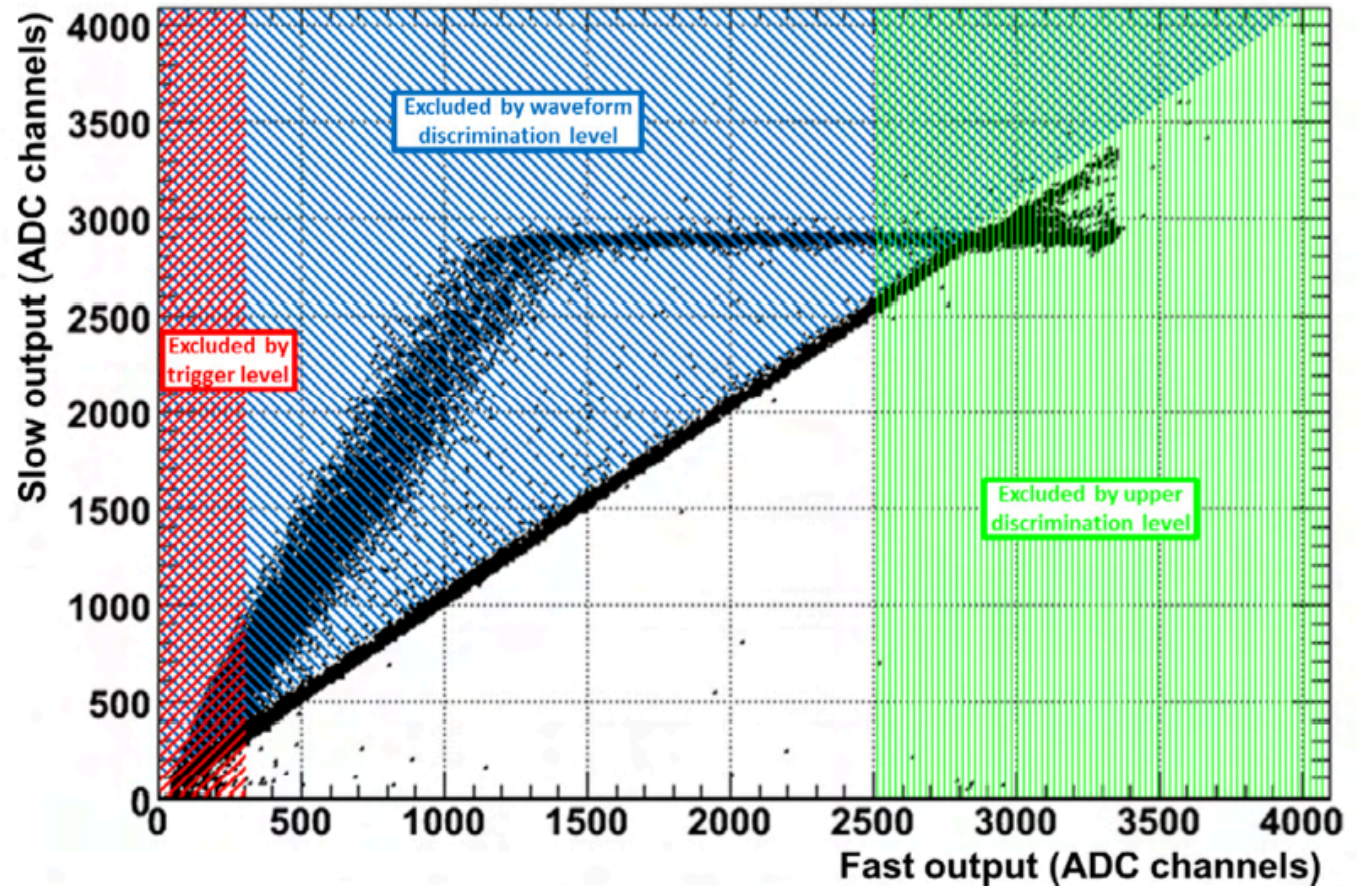
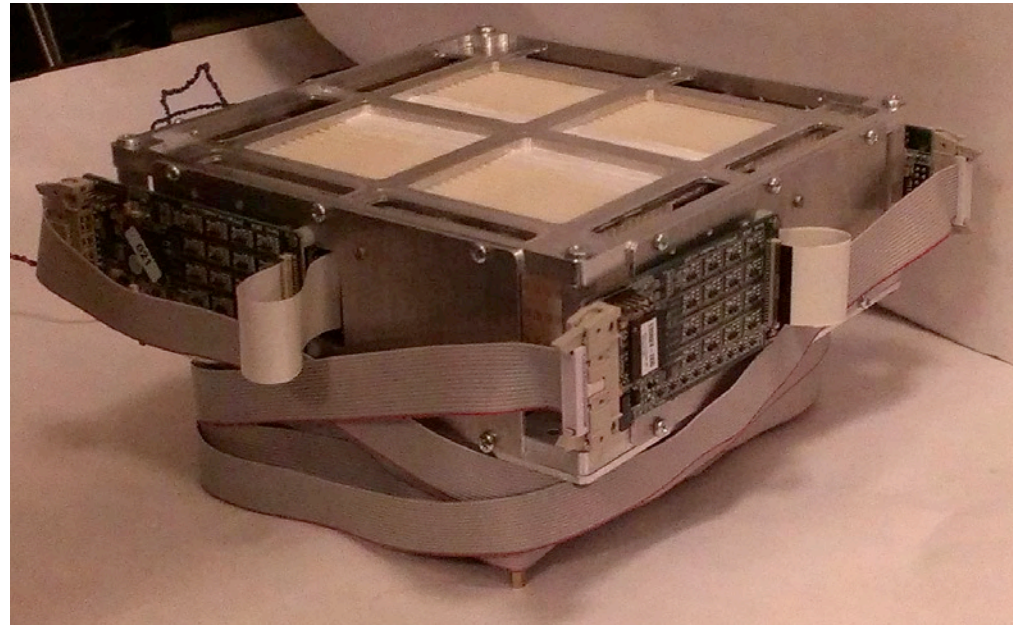
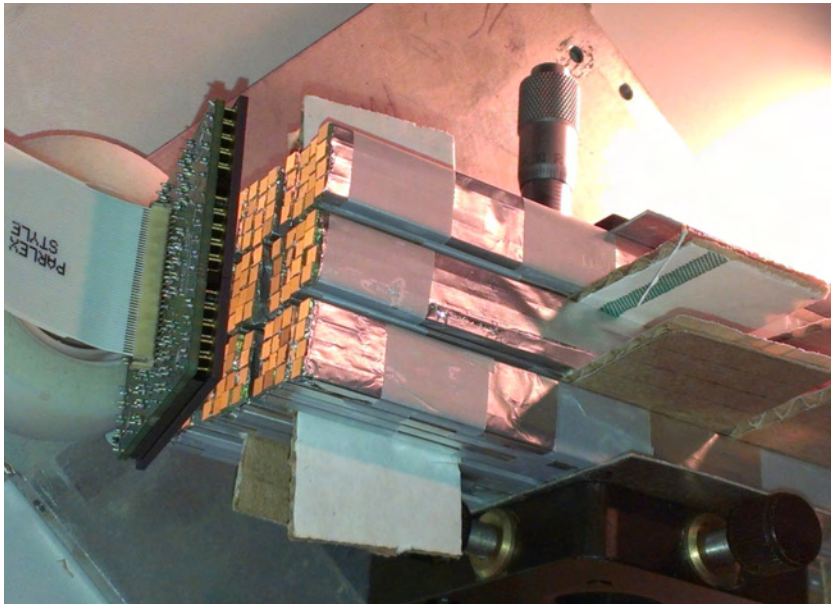


Fig. 4. Photons interacting in the slow scintillator tube or bottom BGO piece (see [Section 2](#)) can be rejected in the data acquisition system using various trigger and threshold settings. The trigger level (red) and upper discrimination (UD) threshold (green) discard noise events and saturated events. The waveform discrimination (WD) threshold (blue) is used to remove events with interactions in the slow or bottom BGO scintillators. The resulting acceptance region corresponds to clean hits which are used for the polarisation analysis. (For interpretation of the references to colour in the text as well as in this figure legend, the reader is referred to the web version of this article.)

Scintillating fibers

Scintillating fibers are widely used as WLS light-guides, but also as a basic detecting material for fine pixellated neutron detectors Iyudin et al. (2015); Koga et al. (2011).

InterSONG



Current sizes range from 0.25 mm to 5 mm square or round cross-sections.

The flexibility of fibers allows them to conform to surface shapes, yielding geometries superior to those of other types of detectors. Examples are detectors for monitoring pipes or barrels.

ISMART-2018, Minsk (RB), 09-12 October, 2018

Scintillators for NanoSats

Mission	Scintillator type	Crystal dimensions	Crystals number	Launch (plan)	PI
SPHiNX	Ce:GAGG EJ-204	60x15x 60x65x65	124 42	2025?	M.Pearce (Sweden)
EIRSAT-1	CeBr3 (Scionix)	25x25x40	1	Selected 2017	L.Hanlon (Ireland)
GRID	Ce:GAGG	38x38x10	4/sat	3 sats 2019	Hua Feng (China)
NanoGam	CeBr3, or Ce:GAGG	2x2x2 cm ³	<40/sat	2-3 sats	L Yacobi (Israel)
BurstCube	CsI (TI)	10x10 cm ²	4/sat	< 6 of 6U CubeSats	J Perkins (USA)
Solar neutron detector	Plastic scint. Ce:GAGG	4x4x64 mm 6x6x6 mm	256 bars 144 pcs	2U CubeSat	Yamaoka& Tajima
Swarm	Ce:GAGG	35x35x5 mm ³	20 pcs/Sat	4 of 3U CubeStas	SI NP

Airborne monitoring of radioactive contamination by unmanned helicopter

A special detection probe based on scintillators, which can be attached to an unmanned helicopter, has been developed in Japan. It can thus monitor the presence of radioactive isotopes, mainly ^{137}Cs , from high in the air, especially in the area of the Fukushima nuclear power plant. The probe must therefore be very light and use little energy. GGAG: Ce^{3+} crystals were selected as suitable scintillation material for gamma radiation detection. The helicopter path was programmed in advance to cover the area of $65 \times 180 \text{ m}^2$ at a height of 10 m for a period of approximately 30 minutes at a speed of 1 m/s and a measuring interval of 10 m. The first attempts prove that in the future this system can serve to quickly and accurately measure the decontamination process, to search for hot zones (local areas with heavily increased radioactivity), and to monitor the spread of ^{137}Cs within the environment around Fukushima; for more information, see *Journal of Nuclear Science and Technology* 2016, 53(12).

Earthquake prediction

After a major earthquake in Tashkent in 1966, and in connection with the observation of the presence of radon in China, a new system has been in place in Japan to build a new earthquake forecasting system based on the monitoring of radon in groundwater. Its concentrations in groundwater are likely to reflect structural changes in bedrock, and it has been found to increase significantly, up to ten times, before large earthquakes. Radon detection in these underground conditions is possible with scintillation detectors that are sufficiently mechanically resistant and can work for years.

Nanocomposite Scintillators

Single-crystal LaBr_3 detectors remain expensive ($\sim \$300 \text{ cm}^{-3}$), and the yields of other materials suffer from difficult crystal growth processes. Los Alamos National Laboratory (LANL) is involved in pioneering research into new gamma-ray detectors that should be capable of energy and timing resolution that approach LaBr_3 , but at a cost similar to non-spectroscopic detectors like plastic.

Recently, the well-known concept of nanocomposite materials has been extended to scintillators, in which nanoparticles of inorganic scintillators are embedded in a transparent organic polymer matrix (McKigney et al. 2007a). To produce a functional material, the size of the inorganic particles must be small enough that the optical transmission properties of the polymer matrix are not affected by the refractive index mismatch of the particles and the polymer. This has been demonstrated with $\text{LaF}_3:\text{Ce}$ nanocomposites (McKigney et al. 2007b). The key to making an optical material with long attenuation length is to produce a nanocomposite comprised of inorganic scintillator particles with diameters of 1 to 5 nm.

In initial work, a photopeak with 16.5% (FWHM) energy resolution at 662 keV using a CeF_3 nanocomposite was achieved. This performance is comparable to that expected from a single crystal of CeF_3 . LANL has also recently synthesized particles of $\text{LaBr}_3:\text{Ce}$ with particle diameters less than 5 nm. Such particles, dispersed at high mass-loading in a polymer matrix, will result in a scintillating material with near-ideal optical properties. Such materials promise the performance of crystalline LaBr_3 at a fraction of the cost.

Conclusion - I

1. The search for new types of “ideal” scintillators is on-going!
2. The study is under way in many countries of Europe, Asia, and in North America.

SCINT 2017 - 14th Int. Conference on Scintillating Materials and their Applications

Monday, 18 September 2017 - Friday, 22 September 2017

[13] Li₂Se(Ag) A New Neutron Sensitive Scintillator

Presenter: RIEDEL, Richard

We report on the discovery of a new neutron sensitive scintillator. Single crystal Li₂Se grown using a flux method and doped with silver was verified to scintillate with exposure to alpha particles (Am-241) and to neutrons (Cf-252). An estimate of the light yield is 2000 photons per neutron capture with a scintillation decay time constant of about 200nsec. Radioluminescence spectra show a strong peak centered near 410nm with a weak secondary peak near 560nm.

ISMART-2018, Minsk (RB), 09-12 October, 2018

Special Anniversary Issue: Professor Jan Czocharlski Year 2013 — Invited Paper

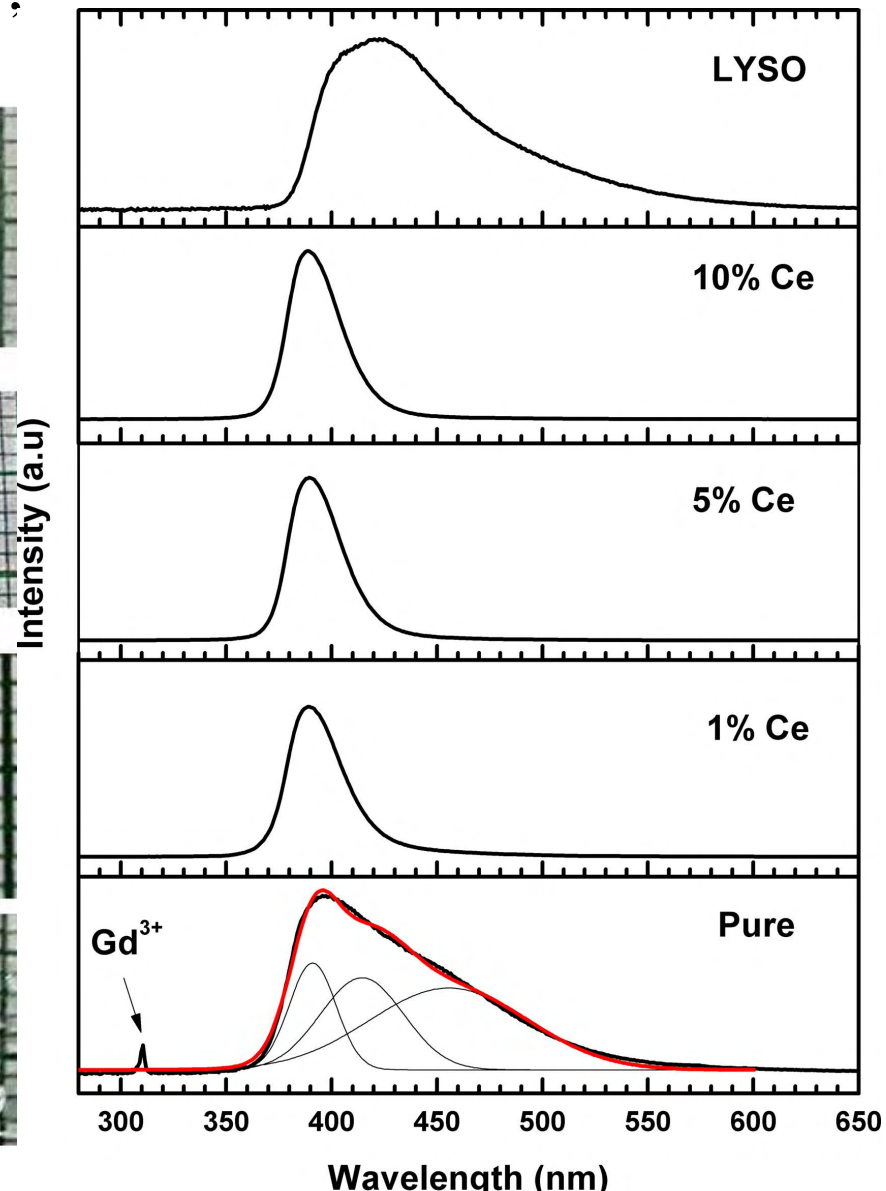
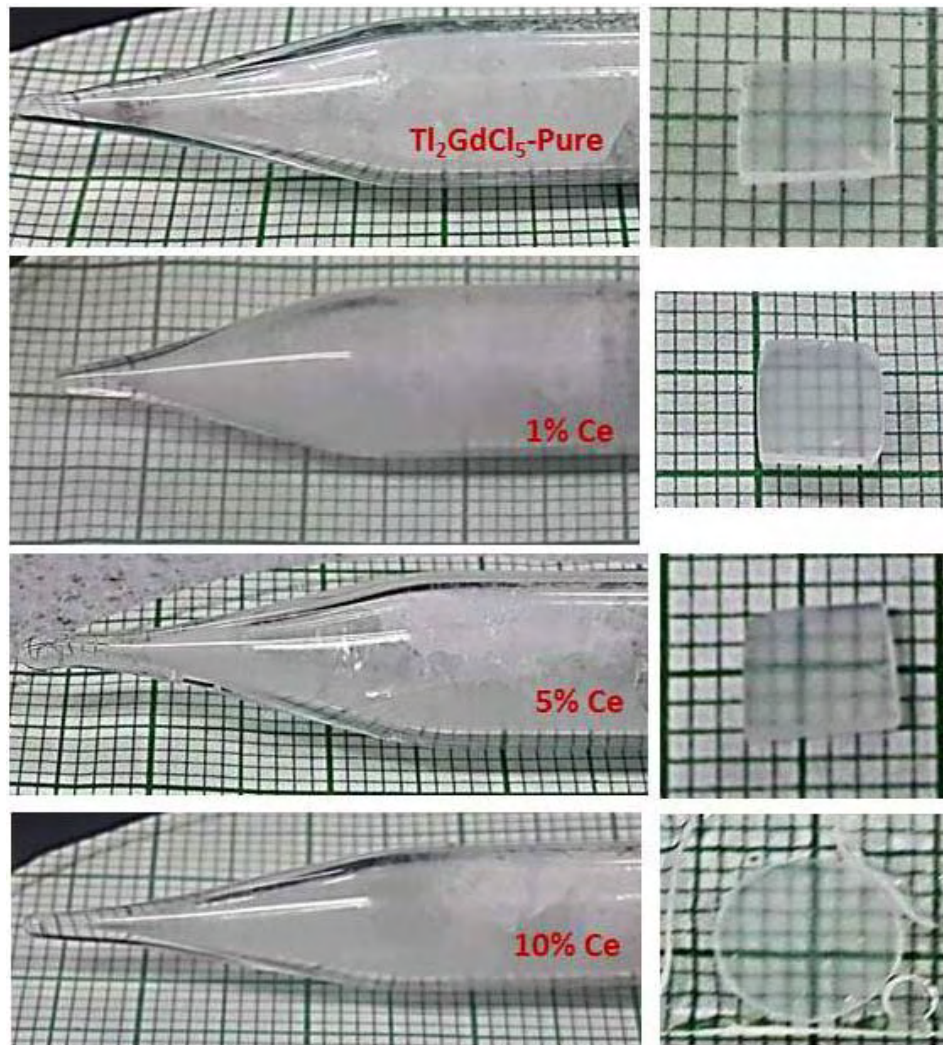
Czocharlski Growth and Properties of Scintillating Crystals

A. YOSHIKAWA^{a,b,*}, V. CHANI^a AND M. NIKL^c^aInstitute for Materials Research, Tohoku University, 2-1-1 Katahira, Aoba-ku, Sendai 980-8577, Japan^bNICHE, Tohoku University, 6-6-10 Aoba, Aramaki, Aoba-ku, Sendai 980-8579, Japan^cInstitute of Physics ASCR, Cukrovarnicka 10, 162 53 Prague, Czech Republic

Crystal	Band gap [eV]	Ce(Pr,Eu) 5 <i>d</i> –4 <i>f</i> em. [nm]	Ce(Pr,Eu) 4 <i>f</i> –5 <i>d</i> abs. [nm]	Ce(Pr,Eu) conc. [mol.%]	Main scint. decay time [ns]	LY (Ph/MeV)	Energy res. at 662 keV [%]
LuAG:Ce [37]	≈ 8	505, 555	202, 215, 227, 346, 448	0.15	55–65 (20–40%)	18,000–26,000	5.5–7
LuAG:Pr [37]	≈ 8	308	Below 190, 239, 284	0.15	20 (20–40%)	16,000–20,000	4.5–6.5
GAGG:Ce [37]	6–6.2	528, 565	235, 342, 439	0.1	88 (90%)	46,000–51,000	4.9–5.5
CdWO ₄ [50]	4.4 ± 0.3 [51]	495	n/a	n/a	5000	27,000	6.6
PbWO ₄ [52, 53]	4.4 [54]	420	n/a	n/a	3–6	200	30–40
LSO:Ce [55]	6.3–6.5	395	Ce1:205–235, 267, 296, 356	0.05–0.1	35	26,000	7.9
GSO:Ce [56]	6.2	430	Ce1:250, 284, 345	0.1	60	12, 500	7.8
YSO:Ce	6.4–6.7	410	Ce1:205–235, 264, 297, 356	0.1	50	24,000	9.3
LYSO:Ce, Ca [57]	6.3–6.5	395	Ce1:205–235, 267, 296, 356	0.05–0.1	39	32,000	8.1
(Lu _{0.6} Gd _{0.4}) ₂ SiO ₅ :Ce [58]	≈ 6.6	415	Ce1:269, 304, 339, 357, 378	0.44	30 (90%)	29,000	6.7
Bi ₄ Ge ₃ O ₁₂	4.96 [59]	480	n/a	n/a	300	8,500	9.0
YAP:Ce	8.8	360	219, 237, 275, 291, 304 [60]	0.15	20–30	21,600	4.6
LuAP:Ce	8.44 [61]	365	216, 231, 278, 294, 308 [60]	0.05	16–20	11,400	9.0
LiCaAlF ₆ :Ce [62]	≈ 12	285	160–174, 227, 244, 271	< 0.01	35	5,000	
LiCaAlF ₆ :Eu [62]	≈ 12	370	200–220, 290–350	< 0.01	1670	(ph./neutron) 40,000	
LaCl ₃ :Ce [63, 64]	7	337, 358	243, 250, 263, 274, 280	10	24(60%)	(ph./neutron) 50,000	3.1
LaBr ₃ :Ce [63, 65]	5.6	355, 390	260, 270, 284, 299, 308	5	16(100%)	70,000	2.6
LuI ₃ :Ce [66, 67]		475, 520	≈ 300, 390, 419	0.5	< 50 ns (50%)	42,000(0.5 μs)	4.7
				2		51,000(10 μs)	–
						58,000(0.5 μs)	
						71,000(10 μs)	

Tl₂GdCl₅ (Ce³⁺): A New Efficient Scintillator for X- and γ -Ray Detection (IEEE TNS, v. 65, p. 2157 (2018))

Gul Rooh , Arshad Khan, H. J. Kim ,
H. Park, and Sunghwan Kim



Conclusion - II

Review

Inorganic scintillating materials and scintillation detectors

By Takayuki YANAGIDA^{*1,†}

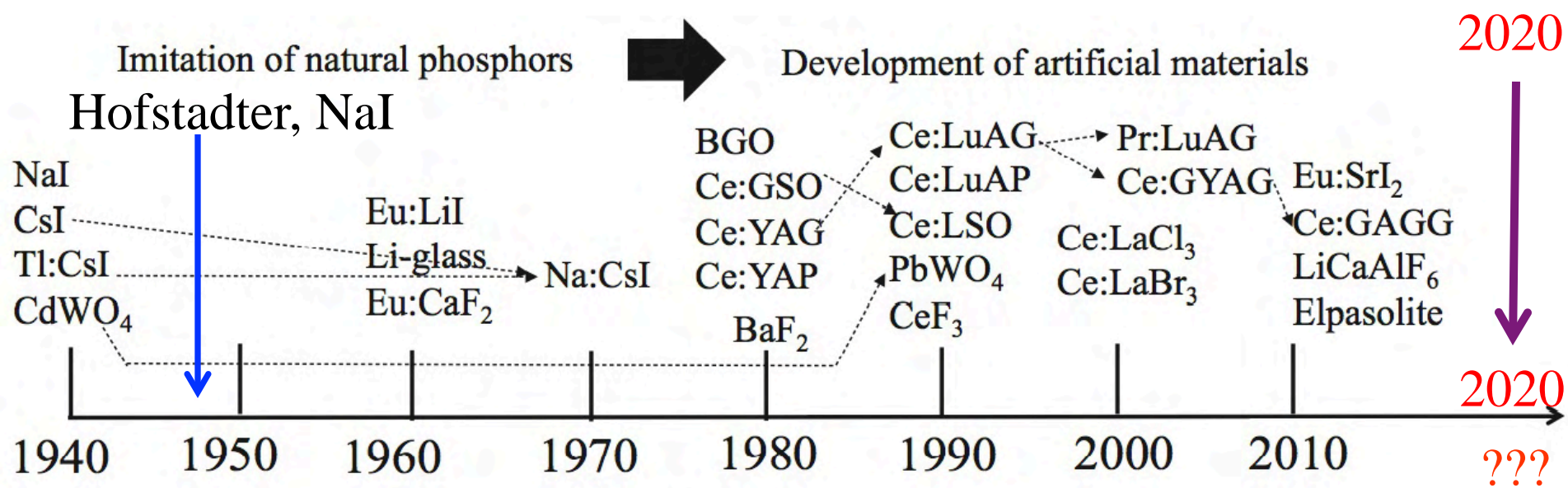


Fig. 8. R&D History of common scintillators. Arrows indicate modifications of materials.

Back-up slides

On sell by C&A Corporation, Japan.

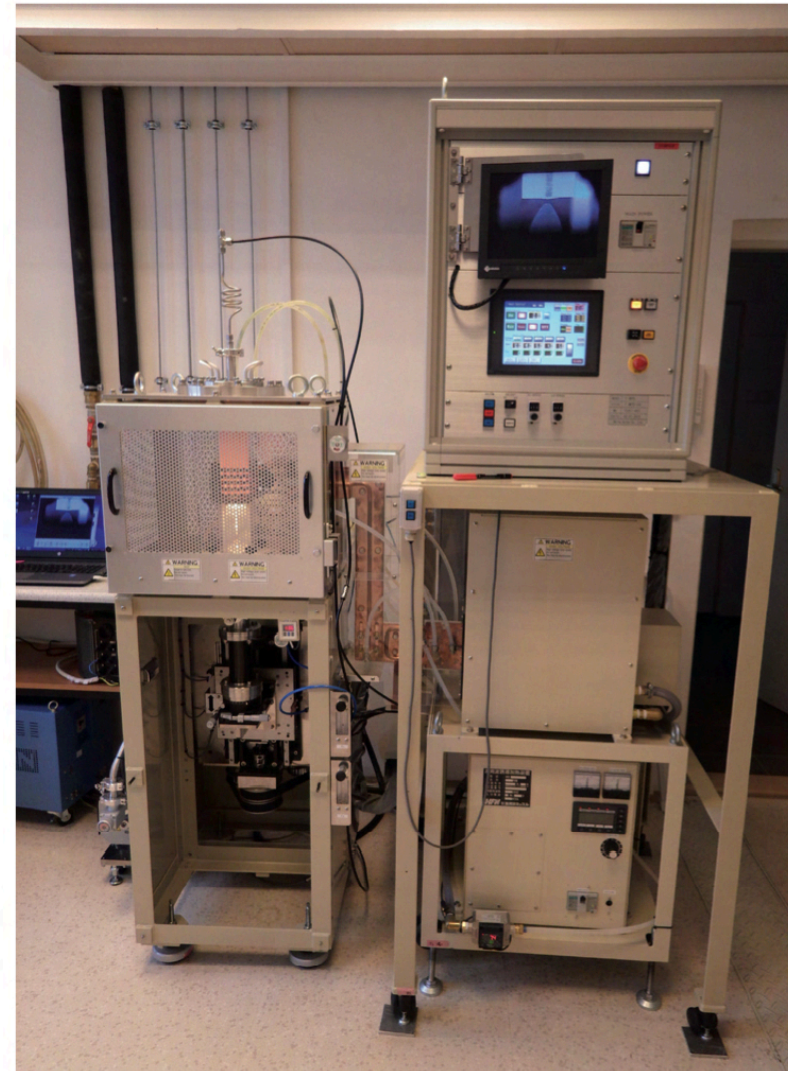
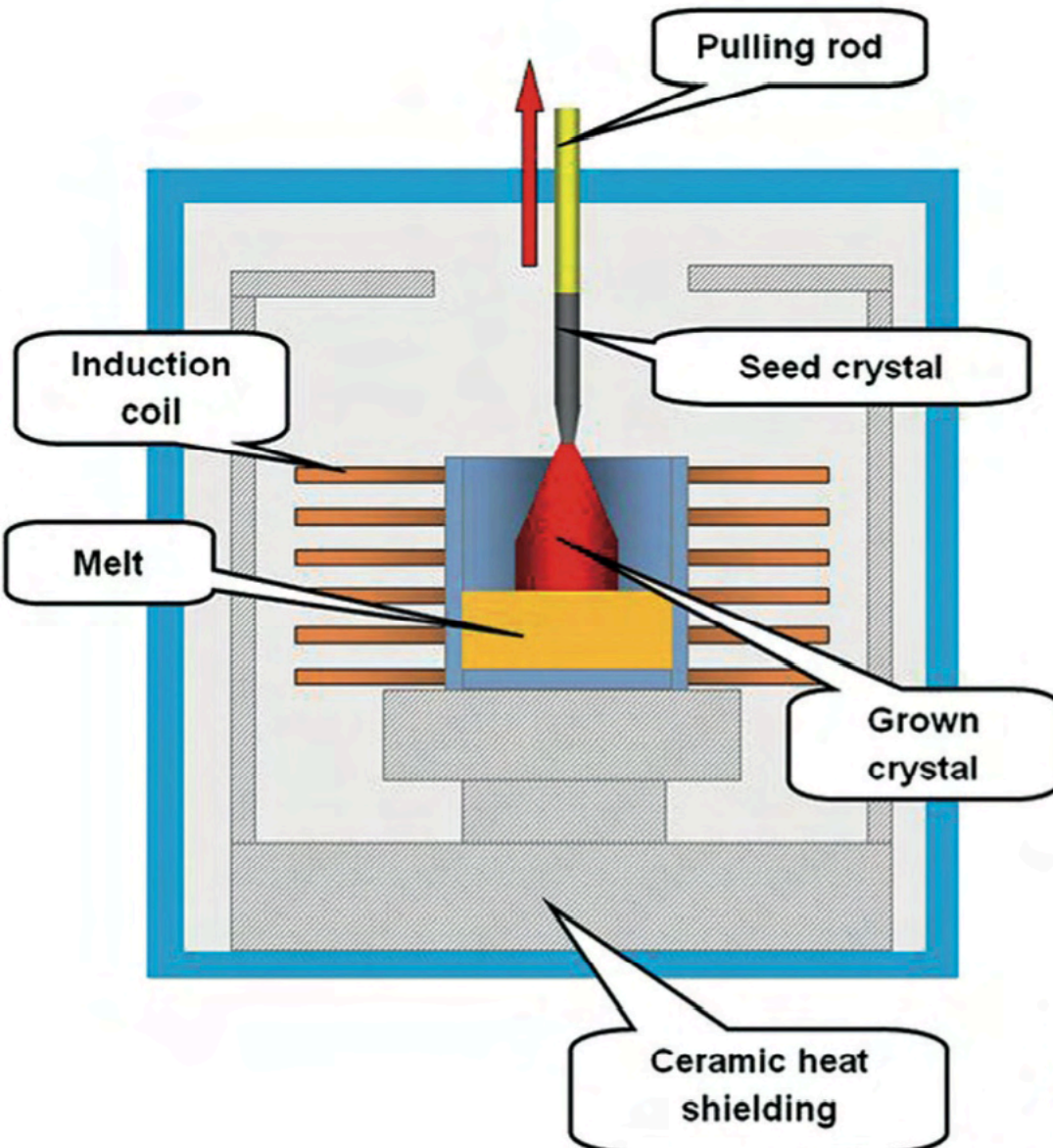


Fig. 3. Schematic of the crystal growth by Czochralski method

Fig. 4. Apparatus for crystal growth by the micro-pulling-down method installed in the Institute of Physics, Czech Academy of Sciences

Micro-pulling-down method

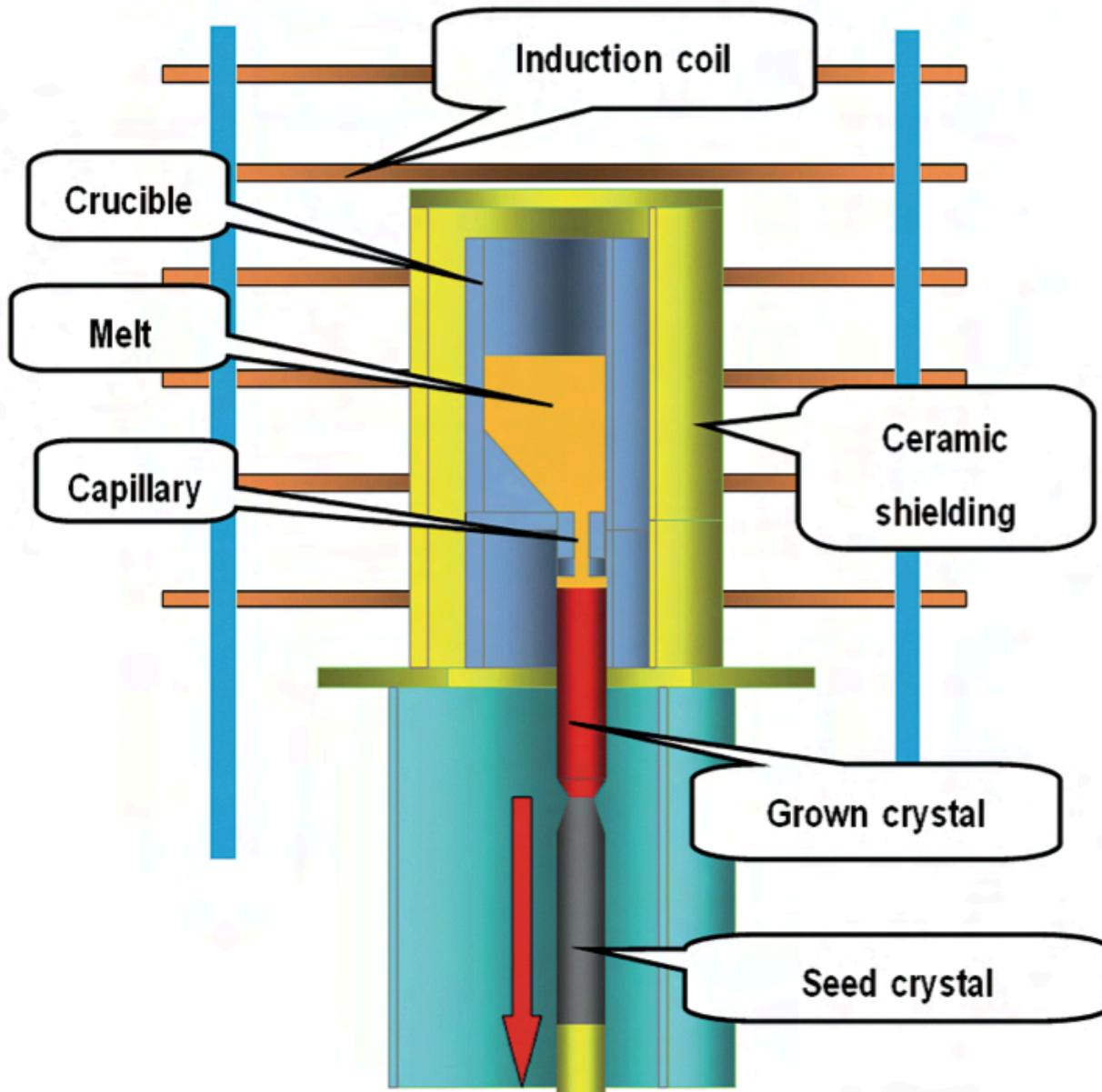


Fig. 5. Schematics of the crystal growth by the micro-pulling-down method

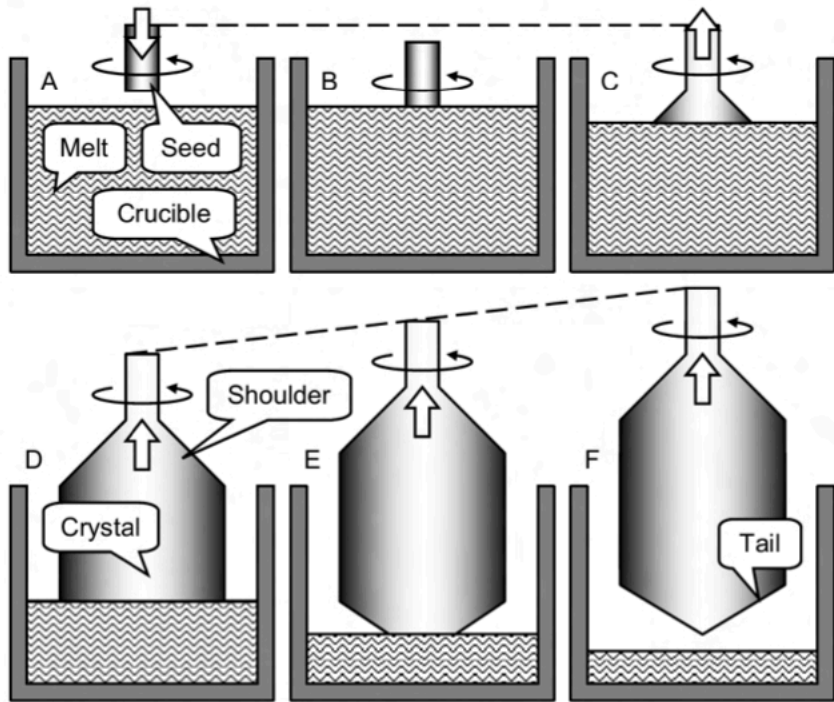


Fig. 1. Phases of typical Czochralski process including (A) approximation of the seed to the overheated melt, (B) immersion of the seed into the melt and their thermal equilibration, (C) pulling of the seed in upward direction with continuous increase of the crystal diameter and shoulder formation, (D) steady state of the pulling of the crystal of constant diameter, (E) ending the growth with continuous diameter decrease, and (F) separation of the crystal from the melt and its following cooling to room temperature.

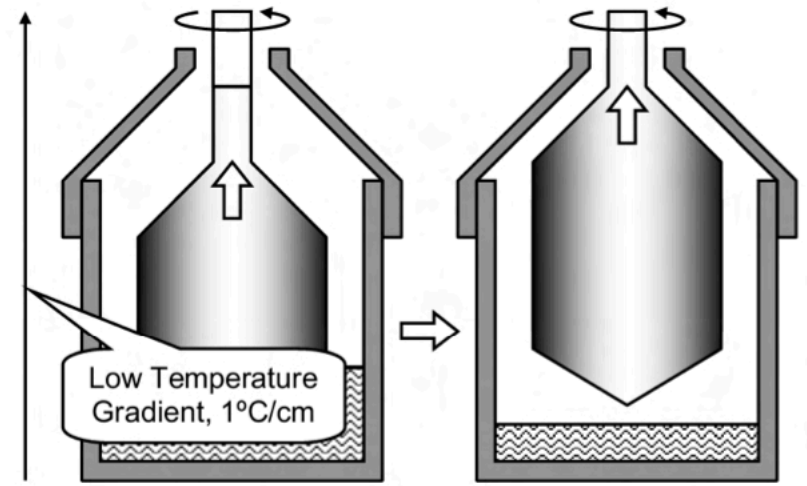


Fig. 5. Growth of the CdWO_4 [15] and $\text{Bi}_4\text{Ge}_3\text{O}_{12}$ [22] crystals by low thermal gradient ($0.1\text{--}1\text{ }^\circ\text{C/cm}$) CZ method.

Czochralski growth parameters.

Item for control	Some factors to control
crucible	material composition, corrosion, melting point, shape and dimensions, contaminations, rotation, displacement, etc.
atmosphere	composition, pressure, flow rate, etc.
melt	composition, starting material treatment, evaporation of constituents, meniscus, corrosion, etc.
seed	structure, composition, orientation, dimensions, shape, etc.
pulling	pulling rate, rotation (rate, acceleration, direction) etc.
thermal aspect	heating source and its power, hot zone design and insulation materials, temperature gradients, automatic diameter control, etc.
cost efficiency	melt solidification fraction, cost of the crucible and the melt ingredients, cost of apparatus, time consumption for the preparation of starting materials, total time of the growth process, etc.